

FAKULTÄT MASCHINENBAU

Master of Science in Manufacturing Technology

Fachgebiet Werkstoffprüftechnik

Prof. Dr.-Ing. habil. Frank Walther

Master Thesis

Development of Acoustic Simulation Method for Brake Squeal based on Experiments in the Test Bench

by

Ömer Anıl Tozkoparan

Registration Number: 181749

Supervisors:

Prof. Dr. –Ing. habil. Frank Walther

Dipl. –Ing. Daniel Hülsbusch

Assist. Prof. Dr. Mehmet İpekoğlu

Submitted on 01.06.2017

**TURKISH-GERMAN UNIVERSITY
INSTITUTE FOR GRADUATE STUDIES IN SCIENCE AND ENGINEERING
MASTER'S PROGRAM IN MECHANICAL ENGINEERING
(MANUFACTURING TECHNOLOGY)
THESIS PRESENTATION PROTOCOL**

18.07.2017

The result of the thesis presentation of Ömer Anıl TOZKOPARAN, who is registered in the joint graduate program Manufacturing Technology between Turkish-German University and Technical University Dortmund with the registration number 1461011101, titled "Development of Acoustic Simulation Method for Brake Squeal based on Experiments in the Test Bench" held on 18.07.2017 at 10.00 is presented below.

Successful

Extension (3 months)

Unsuccessful

Thesis Presentation Committee:

Prof. Dr.-Ing. habil. Frank WALTHER
(Co-advisor)



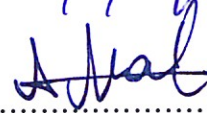
Assist. Prof. Dr. Mehmet İPEKOĞLU
(Co-advisor)



Assoc. Prof. Dr. Güney Güven YAPICI
(Member)



Assist. Prof. Dr. Neşe ARAL
(Member)



Assist. Prof. Dr. Sibel ÖZENLER
(Member)



Master's Thesis

Name: Ömer Anil Tozkoparan
Supervisors: Prof. Dr.-Ing. Frank Walther, Dipl.-Ing. Daniel Hülsbusch
Subject: Development of Acoustic Simulation Method for Brake Squeal based on Experiments in the Test Bench

Brake squeal is a friction-induced high frequency (beyond 1 kHz) noise problem that is observed in automotive disc brake systems. As opposed to other friction-induced noise and vibration problems, it is a dynamic instability phenomenon and usually observed at low operating speeds. Based on minimal order mathematical models, the following mechanisms are believed to lead squeal noise: 1) stick-slip oscillations due to negative damping effect; 2) sprag-slip; 3) mode coupling/splitting; 4) self-excited vibrations at constant friction coefficient; 5) hammering. Due to one of these mechanisms, an unstable mode of the physical system gets excited hence generates squeal noise.

General Concept of the Project to be proposed

Modal Tests: In order to understand the physical system, first modal tests will be performed and eigenfrequencies and modes will be determined. These tests will be executed by hitting the system by an impact hammer and collecting acceleration data at several locations on the system. Firstly, these tests will be done on component level, i.e. components of the brake system such as disc, pad caliper etc. Then, the entire brake system assembly will be tested (see laboratory experiments). As an outcome of these studies, the system along with its components will be understood in terms of their modal properties. Matlab will be used for mode shape visualization.

Computational Studies: A computational model of the brake system will be developed and its modal properties will also be calculated from the computational solution of the complex eigenvalue problem in Abaqus. These eigenvalues will be compared by the experimental modal test results and the FE model will be updated. After validating the FE model, it will be solved for different operational parameter sets and the unstable modes will be determined. These parameter sets will also be validated with actual test results.

Laboratory Experiments: In order to validate the computational model, a laboratory test system as schematically shown below will be designed and built. On this setup, brake system will be attached on a supporting structure that is in a semi-anechoic room, and will be driven by an electric motor that locates next room. Hence, the noise from the driving system will be isolated from the measuring signals. Experiments will be run at different operational conditions such as brake pressure, speed, etc. and squeal phenomenon will be generated at the laboratory environment. Based on the experimental measurements, the computational model will be validated afterwards.

Prototype Design: After validating the computational model with experiments, new ideas to treat squeal problem on the brake system will be developed. According to these ideas, computational model will be modified and similar computational work will be done to see if the solution is effective. Then, these modifications will be applied to the physical system, and experimental cases will be rerun on the modified system. As a result, it is expected to have a new prototype brake system that has a better squeal performance.

Dortmund, 01.11.2016



(Prof. Dr.-Ing. habil. Frank Walther)



Abstract

Brake squeal is a comfort problem in consequence of the increase in the customer expectations, although it does not cause a safety hazard. The chief goal of this thesis is to investigate brake squeal in the brake system of the light commercial vehicle. In the scope of the thesis, the studies were divided into two main groups: Experimental studies and finite element (FE) modelling.

Experimental studies consist of performing experimental modal analysis (EMA) and conducting squeal tests in the test bench. First, experimental modal analysis (EMA) was utilized to obtain modal parameters of the brake components (disc, brake pad, caliper and carrier) and the assembly. By utilization of the impact hammer and acquiring the acceleration data at measurement points on the structures, the mode shapes and natural frequencies of the components and the assembly were attained. Second, the squeal tests were conducted in semi-anechoic room by performing different levels of brake pressure and speed. During the experiments, acceleration and sound pressure signals were measured to attain the mechanic and acoustic modes of the system.

Finite element modelling consists of building the FE model of the brake system, tuning the modal parameters of the brake components according to the experiment results and building a new simulation method to investigate squeal. First, the generated FE model of each brake component was validated with experiment results in terms of mode shape and natural frequency. The FE model of the brake assembly was built and the initial step of the simulation method was completed. The parameters which are friction, contact, braking pressure, rotational speed of the disc and other working conditions were defined in the simulations. Hence, the FE model of the brake system and the simulation method were developed and validated based on the experimental results.

Finally, after the parameters which lead to squeal were defined, a design proposal to suppress squeal was made considering the applicability, cost and other criteria. Two structural modifications on the friction material were proposed and investigated in the simulation model. Two prototypes were obtained by applying the determined structural modifications in the machine shop. Afterwards, the squeal tests were performed by employing these prototypes. The achieved improvements for the reduction of squeal in simulations were observed likewise in the squeal tests.

In conclusion, the developed simulation method well predicts the dominant squeal frequency measured in experiments. Moreover, the suggested structural modifications developed with the simulation model show promising results for the squeal treatment.

Table of Contents

Abstract.....	iii
Abbreviations and Symbols	vi
1 Introduction	7
1.1 The Basics of Disc Brake	7
1.2 Brake Noises	8
1.3 Common Investigations.....	10
1.4 Contribution of Thesis	10
1.5 Outline	11
2 State of the Art.....	13
2.1 Definitions and Basics.....	13
2.1.1 Experimental Modal Analysis	13
2.1.2 FE Modelling	16
2.1.3 Instability Analysis of the Brake System via CEA	18
2.2 Analytical Investigations	18
2.2.1 Stick Slip	19
2.2.2 Sprag Slip.....	20
2.2.3 Mode Coupling.....	21
2.3 Experimental Investigations	22
2.4 Finite Element Approach	23
2.5 Treatments for Disc Brake Squeal	24
3 Experimental Modal Analysis.....	25
3.1 Introduction.....	25
3.2 Experimental Setup.....	25
3.3 Modal Testing of Disc Brake Components	27
3.3.1 Brake Disc.....	27
3.3.2 Brake Pad	29
3.3.3 Carrier	31
3.3.1 Caliper.....	32

3.4	Modal Testing of Assembly	35
4	Numerical Modal Analysis.....	36
4.1	Introduction.....	36
4.2	Validation of Disc Brake Components.....	37
4.2.1	Brake Disc.....	38
4.2.2	Brake Pad	39
4.2.3	Carrier	41
4.2.4	Caliper.....	42
4.3	Validation of Brake Assembly.....	45
5	Investigation of Disc Brake Squeal	46
5.1	Introduction.....	46
5.2	Experimental Studies of Disc Brake Squeal.....	46
5.2.1	Methodology and Experimental Setup	46
5.2.2	Results	49
5.3	Complex Eigenvalue Analysis	53
5.3.1	Brake Squeal Analysis Using FEM	53
5.3.2	Results	53
6	Design Modifications and Sensitivity Analysis	56
6.1	Effect of Brake Pressure	56
6.2	Effect of Elastic Modulus of the Friction Material	57
6.3	Geometry Modifications of the Brake Pad.....	58
7	Conclusions	60
8	Bibliography	62
9	List of Figures	65
10	List of Tables	67

Abbreviations and Symbols

Abbreviation	Designation
EMA	Experimental Modal Analysis
CEA	Complex Eigenvalue Analysis
FE	Finite Element
FEM	Finite Element Method
DTA	Dynamic Transient Analysis
FFT	Fast Fourier Transform
FRF	Frequency Response Function
DAQ	Data Acquisition
R&D	Research and Development
DoE	Design of Experiment

Symbols	Unit	Designation
$\gamma(\omega)^2$	-	Coherence function
ω	Hz	Natural frequency
$H(\omega)$		Transfer function
$X(\omega)$		Output spectrum
$F(\omega)$		Input spectrum
μ		Coefficient of friction

1 Introduction

The brake systems are utilized either to decelerate the vehicle or to maintain the velocity. Hence, performance and safety are the important criteria to evaluate the quality of the brake system. However, the brake comfort has gained importance from the view of the customers who suppose their brakes are broken when they hear brake noise. Therefore, the investigations of squeal have increased in recent years.

The summarized contents of this study are given in this chapter. First, the fundamentals of disc brakes are introduced shortly. Second, the classification of the brake noises is expressed and the importance of brake squeal from the viewpoint of automobile manufacturers is explained. Third, the approaches on the evaluation of brake squeal are introduced shortly. Then, the aim and objectives of this thesis are presented. Finally, the outline of this study is given to enable readers to follow this work conveniently.

1.1 The Basics of Disc Brake

A modern disc brake is composed of essential components such as caliper, brake disc(rotor), brake pad, piston, carrier, caliper, knuckle, axle hub and a hydraulic line which provides pressurized fluid. In Industry, different caliper designs are available, however in this section the structure and working principle of the calipers are explained shortly. To search detailed information about calipers and automotive braking systems helpful sources are available in literature [Har98] [Kin03] [Hal16].

The brake disc has rigid connection with the axle hub rotated by drive shaft. The braking is realised by the generation of the braking force on the brake disc. The brake pads, which mainly consist of a back plate and a friction material, apply force against the brake disc. The actuation of the pads depends on the caliper design, which has fixed and sliding types (Figure1.1).

In fixed caliper, on both inboard and outboard sides have pistons actuated by pressurized fluid so that the pistons apply force on the brake pads which generate torque on the disc is stationary (Figure 1.1.a). On the other hand, a sliding caliper contains one or more piston and slides over the guiding pins as the braking is performed. When a piston moves to the disc, the caliper moves in opposite direction by means of the reaction forces. Hence, the outboard pad applies torque on the disc. The piston applies force on the in board pad which applies also torque on the disc.

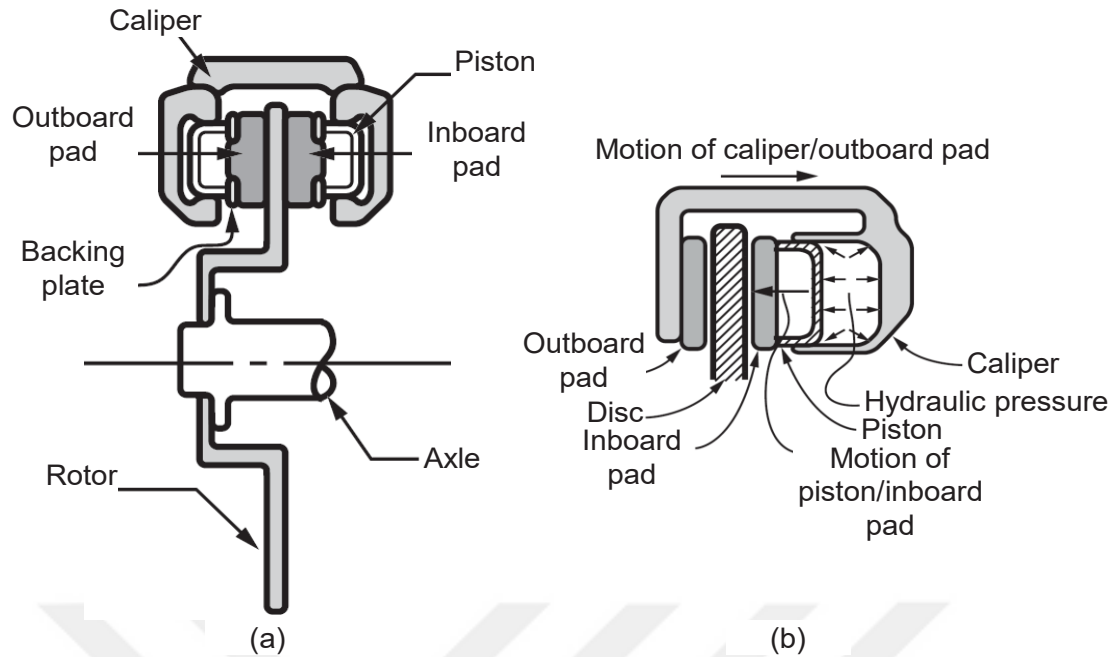


Figure 1.1: Two main caliper design are shown schematically a) Fixed caliper b) sliding caliper. This figure is adapted from [Kin03].

Safety and performance are the key factors taken into account by the brake engineers concerning the research and development of the brake systems. After the targets of these factors are fulfilled a brake system is investigated in terms of noise and vibration brake comfort. To select or develop a brake system regarding safety and performance is not an aim of this thesis. In this study, the chief goal is developing a simulation model to make consistent predictions for the dynamic instabilities of the brake system which have a propensity of brake noises. will be utilized to work on the brake system in further R&D processes. The success of the simulation model is measured with its correlation with experiments. By employing the successful simulation model MB Türk A.Ş. will eliminate the brake noise at the design stage of the new brake systems.

1.2 Brake Noises

Noise and vibration are the form of instabilities observed in the brake systems. Generally, two type of classification are done for these instabilities. The first classification is regarded as traditional classification which categorizes the instabilities according to their fundamental frequencies, where the instabilities which are below a certain limit (100, 500 or 1,000Hz) are named as judder or hum and the ones above this limit named squeal [Jac03]. On the other hand, the second classification named as phenomenological classification sorts the instabilities based on the physical mechanisms causing these instabilities [Jac03]. This classification consists of three groups as forced vibrations (judder, hum), vibrations mainly caused by friction

features (creep groan, dynamic groan and moan) and vibrations mainly caused by resonance of the brake components (squeal and wire brush) [Jac03].

Judder is a low frequency instability and has a relation with wheel speed. It occurs mostly below 200 Hz and is originated from the geometric variations of the friction disc. The reasons for these variations are sorted as corrosion, uneven wear of the disc, friction coefficient variations caused by uneven coating on rotor surface, plastic deformation of the disc caused by thermal effects. Because of this torsional vibrations occurs at a frequency which is proportional to wheel speed [Day14]. Although judder is important issue, it is not studied in the scope of this work.

Squeal, which is regarded as high frequency noise problem, is most investigated topic compared to other noise and vibration problems occurring in brake systems [Jac03] [Pap02]. This noise occurs due to the dynamic instabilities caused by friction and is observed between 1 and 16 kHz. The annoying vibrations are perceived by the people as acoustic noise rather than structural noise, which affects the comfort of the drivers and other people. The main reason of squeal is that one of the natural frequency of the brake system is excited by a physical mechanism, hence the brake system becomes unstable. The main physical mechanisms can be sorted as follows 1) stick-slip 2) sprag-slip 3) self-excited vibrations with constant friction coefficient 4) mode coupling and 5) hammering [Kin03] [Rhe89]. In addition, Dai and Lim [Dai08] classified the brake noises in terms of annoyance based on the statements of drivers, fundamental frequency and type of excitation (Figure 1.2). In addition to squeal and judder other brake noises such as Howl and Wire brush are also illustrated. In the scope of this work, these noises are not discussed. The detailed information about these noises can be found in literature [Dai08] [Day14].

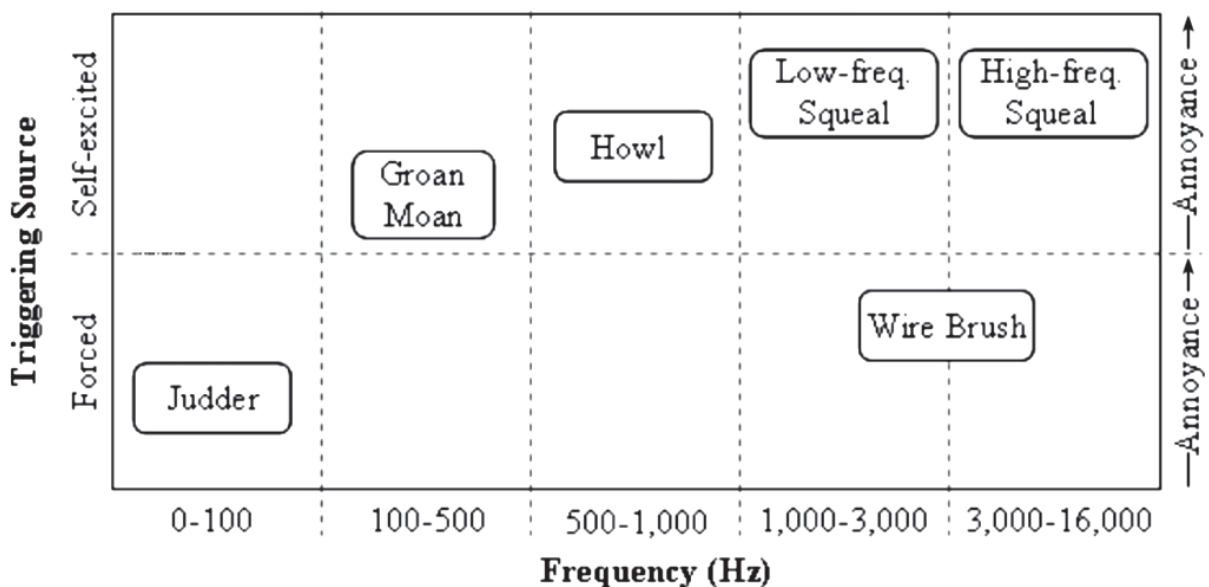


Figure 1.2: The classification of brake noise [Dai08].

In Figure 1.2, it can be clearly seen that the annoyance level of squeal is higher than the other noises. Moreover, when customers hear brake squeal, they suppose that it is an indication for a defective brake system and make warranty claims for their brake systems actually working well regarding performance and safety. Hence, the investigations have been conducting by auto manufactures to defeat brake squeal.

1.3 Common Investigations

In literature, the studies on brake squeal are divided three main approaches. Although these approaches are presented in detail in chapter 2, in this subchapter brief overviews for each one are given. The first one is analytical approach adopted to study the mechanisms of squeal with low order models, which allow to study on the stability considering appearance of the squeal mechanisms. The second approach is experimental approach chosen to investigate squeal by dynamometer tests and on road tests of a vehicle. In doing so, the data of different tests conducted with operational conditions are collected and a conclusion is made. The third one is Finite Element (FE) approach utilized to study on stability of brake system with large degree of freedom. In industry, two main FE approaches available to predict brake squeal. The first one is Dynamic Transient Analysis (DTA) making possible to integrate time varying properties in simulation. However, the main disadvantage of this approach is that it requires long computing time. The second one is Complex Eigenvalue Analysis (CEA) evaluating the unstable modes of the system in a single run with less computing time compared to DTA. CEA is most preferred FE approach in brake industry because it provides convenience to obtain unstable modes. The aim of brake engineers is making structural modifications to prevent squeal. Therefore, calculating unstable modes in short time is important for them. In this study, CEA is employed due to aforementioned reasons.

1.4 Contribution of This Thesis

The chief aim of this thesis is developing a simulation method to predict instabilities of the brake system based on squeal tests in test bench. In order to do so, experimental analysis and Finite Element Method (FEM) are utilized to study the dynamic instability and its corresponding brake noise regarded squeal.

The major contributions of this thesis are as follows:

- Performed detailed modal testing for each brake components (disc, caliper, carrier, brake pad)
- Constructed FE models of the brake components considering mesh type and mesh size.
- Updated the material parameters of the FE models based on the modal testing results

- Determination of the operational conditions in test bench to obtain squeal frequencies observed in field measurements of the vehicle.
- Repetition of the squeal tests with determined operational conditions till the repeatability and stability of the squeal tests ensured.
- Construction of the FE Model of the brake system by assembling the brake components, whose material parameters are updated via the comparison of modal testing and real eigenvalue analysis
- Modelling of the simulation method regarding the connection types and interactions in between the components in test bench
- Employing Complex Eigenvalue Analysis (CEA) with operational conditions of the real brake system to predict the instabilities of the brake assembly, after the simulation model is obtained without converge problem.
- Aiming to reduce instability in CEA with two new pad design modifications. The prototypes of these design modifications were made. The improvements attained in CEA are also observed in experiments in the test bench.

1.5 Outline

In this subchapter, the overviews of the all succeeding chapters are explained briefly in order to draw the picture of the thesis, which enable the readers to follow the contents conveniently.

2. State of the Art: This chapter starts with explanations of some basics needed to follow the logic of succeeding chapters. Then, brake squeal mechanisms are explained briefly. Subsequently, the approaches conducted to investigate the brake squeal are presented. This chapter ends with short overview of the treatments performed to suppress brake squeal.

3. Experimental Modal Analysis: In this chapter, EMA is performed not only at component level but also at assembly level. Firstly, the natural frequencies and mode shapes of the brake components are extracted by utilizing rowing hammer technique. Secondly, modal testing at assembly level is performed with the measurement points at friction disc.

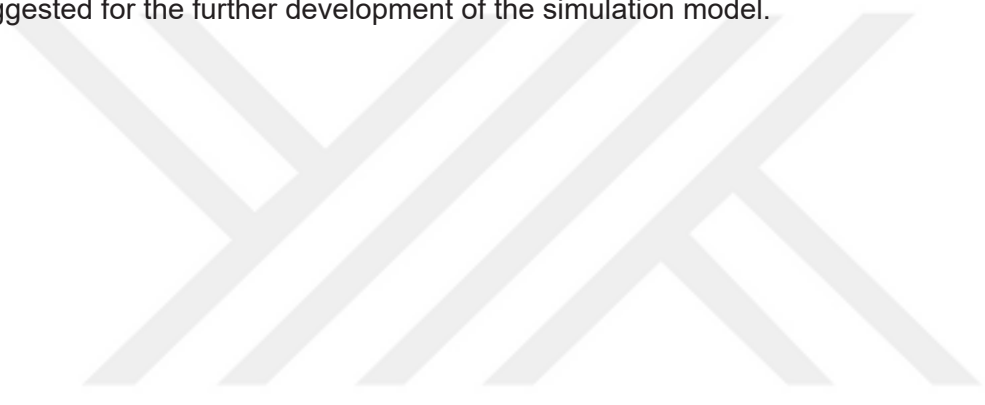
4. Numerical Modal Analysis: The structure of this chapter is similar with previous chapter, which starts with component level and ends with assembly level. Real eigenvalue analysis is executed by a commercial FE solver for component level as well as assembly level. The evaluated natural frequencies and mode shapes of each structure are compared with experimental results attained in chapter 3.

5. Investigation of Disc Brake Squeal: This chapter starts with an introduction of test bench employed for squeal tests. After conducting controlled controlled experiments, the operational

conditions which lead to squeal are determined. The test results are discussed and a dominant squeal frequency determined. Afterwards, CEA is utilized by using real operational conditions attained in squeal tests to predict the instability of the brake system. The predicted instabilities and squeal results are discussed.

6. Design Modification and Sensitivity Analysis: In this chapter, a possible squeal treatment performed by modifying the geometry of the friction material is proposed. First, the effects of the mentioned modifications on stability of the brake system is studied within the framework of the FE simulation. Then, the same modifications are applied on real brake pads and squeal tests are conducted. These test results are compared with the outcomes achieved in CEA.

7. Conclusion: This chapter summarize the aim and all the objectives of this thesis. The methods applied to build a consistent simulation model are discussed. Future works are suggested for the further development of the simulation model.



2 State of the Art

2.1 Definitions and Basics

The purpose of this section is to explain some the terms and fundamental information which are used in proceeding chapters.

2.1.1 Experimental Modal Analysis

The Experimental Modal Analysis (EMA) enables to understand the dynamic behavior of a structure regarding its natural frequencies, mode shapes and modal damping. Hence, performing a modal test on a brake component is crucial to obtain the dynamic parameters which are referenced in the validation of a corresponding FE model. A modal test starts with a mechanical excitation of a structure by means of an impact hammer or an electromagnetic shaker [Ewi00]. The response of the structure is recorded on the basis of its motion parameters, such as displacement, velocity or acceleration. Generally, an accelerometer is used as a transducer in modal testing due to its good linearity, wide frequency range, low weight and simple mounting techniques [Døs88].

The analog signals of the experimental modal analysis must be processed by a data acquisition system (DAQ) to interpret the dynamic behavior of a structure adequately. The basic steps of the data acquisition for impact testing are shown in Figure 2.1. The steps are explained briefly as follows [Avi14] :

- 1) The input signal acquired by an excitation device and the output signal acquired by a sensor are processed by using a low-pass filter to eliminate the influence of high frequencies and consequently to prevent the Aliasing effect.
- 2) The data is converted from analog to digital form by using an analog to digital converter (ADC). The data is digitized by defining a proper sample rate to convert analog data into discrete digital dataset. The sample rate is set at least the double of the maximum frequency of interest, as defined by the low-pass filter [Ewi00].
- 3) The digitized data is processed by applying a window function which is necessary to eliminate the noises in the Fourier transformation step due to leakage.
- 4) The data is converted from time-amplitude into frequency-amplitude domain by means of a Fast Fourier Transform (FFT) and linear spectrums of the input and output signals are obtained.
- 5) The experiments are repeated for statistical evaluation. The input power spectrum (G_{xx}), output power spectrum (G_{yy}) and cross power spectrum (G_{yx}) are obtained from averaged data. Finally, the Frequency Response Function (FRF) and the Coherence Function (CF) are computed.

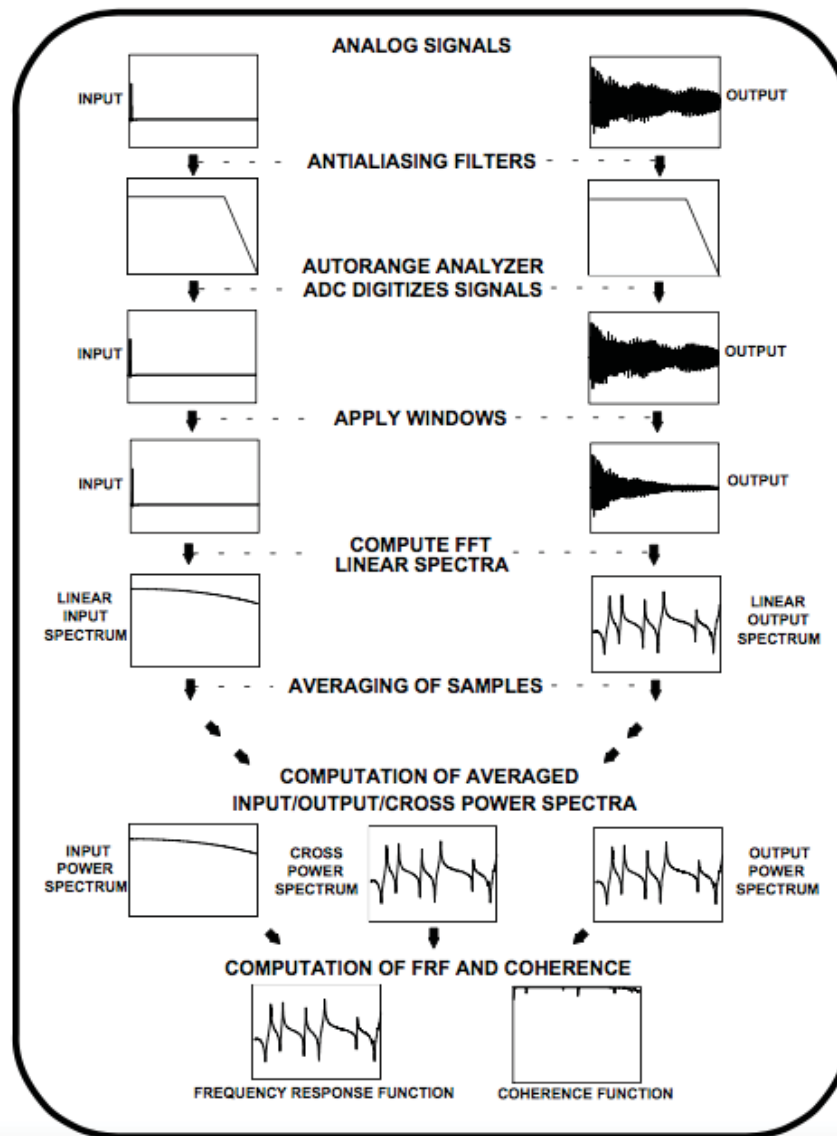


Figure 2.1: The flow diagram of signal processing for impact test [Avi14].

To express the dynamic behavior of a structure as a mathematical function, the complex ratio of output spectrum, $X(\omega)$, and input spectrum, $F(\omega)$, is calculated. This ratio is called the Frequency Response Function (FRF), $H(\omega)$, which is expressed as $H(\omega) = X(\omega) / F(\omega)$. The Figure 2.2 is adapted from [Døs88].

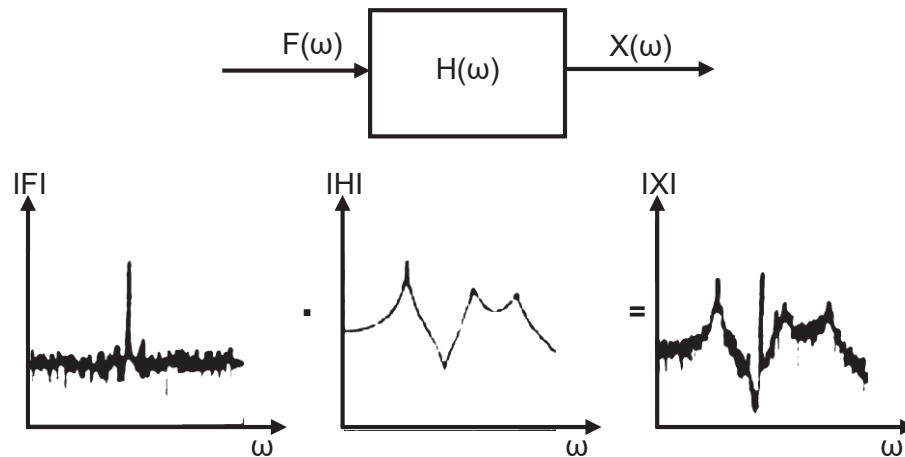


Figure 2.2: Output spectrum is obtained by linear multiplication of input spectrum and FRF. This figure is adapted from [Døs88].

A sinusoidal output motion of the concerning structure is obtained through the multiplication of a sinusoidal input force of the same frequency with the FRF. The peaks in either the FRF or the output spectrum represent the natural frequencies of the structure. The sharpness of these peaks give a hint about the damping ratio at the corresponding natural frequency. A low damping ratio causes sharp peaks whilst a high damping ratio results in smoother peaks [Ewi00]. Modal testing is a linear approach which provides a symmetric FRF matrix (Figure 2.3). The FRF can be described as a matrix H_{ij} , where i stands for response point whilst j denotes excitation point. For instance, the FRF(H_{21}), obtained by an excitation at "point 1" and analysis of the response at "point 2" is identical with the FRF(H_{12}) which is computed from the response at "point 1" after excitation at "point 2". This feature of modal testing is known as reciprocity [Avi14].

When both the excitation and the measurement are conducted at the same location and the response is measured in the same direction of the excitation, this point is denoted a drive point [Avi14]. The FRFs of the driving points (H_{11} , H_{22} , H_{33}) can be seen in Figure 2.3. Besides the peaks at resonance frequencies, the valleys seen between the peaks in driving point measurements are called antiresonance [Avi14].

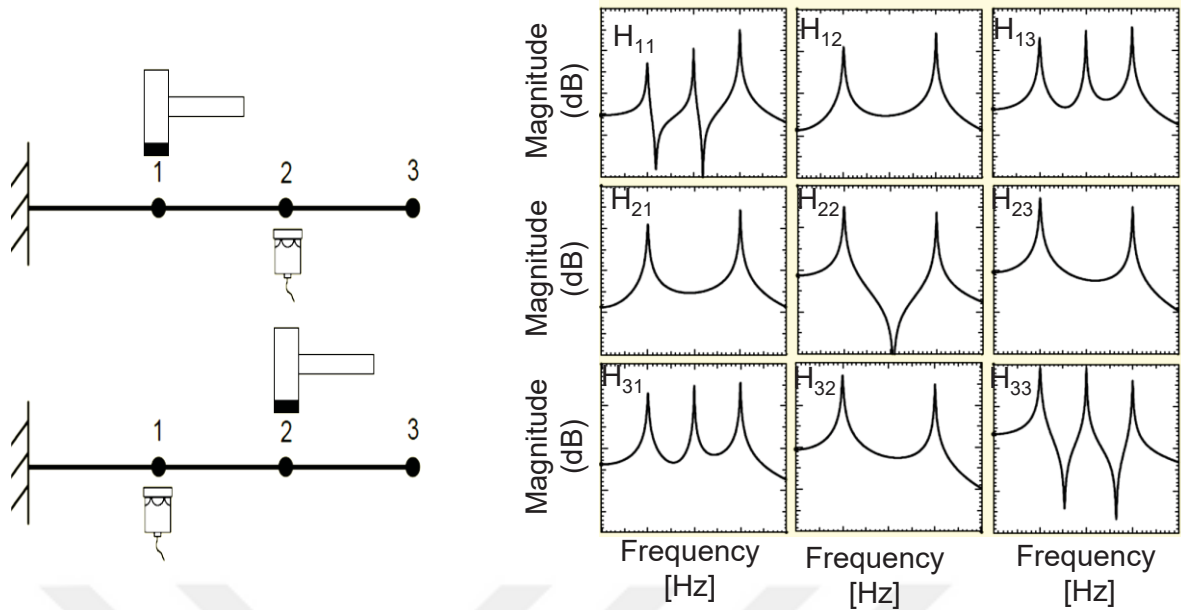


Figure 2.3: FRFs of a cantilever beam obtained at different excitation and response points. This figure is adapted from [Avi14].

To assess the quality of each FRF measurement a so-called Coherence Function ($\gamma(\omega)^2$) is computed. This function is based on the linearity between the input and output signals. If one of the auto spectrum includes noise, the quality of FRF decreases in consequence of deteriorations in coherence function. The coherence level range is between 0 and 1. A value of 1 equals no noise in measurement and a measurement with fully noise is represented by a value of 0. The equation of the coherence function $\gamma(\omega)^2$ is given as follows [Døs88]:

$$\gamma(\omega)^2 \equiv \frac{|G_{YX}(\omega)|^2}{G_{XX}(\omega) \cdot G_{YY}(\omega)} \quad 0 \leq \gamma(\omega)^2 \leq 1 \quad (2.1)$$

Where ω stands for a natural frequency, G_{XX} denotes the input spectrum; G_{YY} represents the output spectrum and G_{YX} symbolizes the cross spectrum. For a more detailed discussion about modal analysis see the articles of Peter Avitabile [Avi14] and the book written by D.J. Ewins [Ewi00].

2.1.2 FE Modelling

In Abaqus, the designation of an element provides information about the properties of the element. For instance, the element type C3D8 denotes a 3-dimensional continuum element and has 8 nodes. An element type C3D8I represents the developed version of an element type C3D8 and is used to suppress the shear locking which is a kinematic problem of the linear elements in FEM. Type C3D8I is generally preferred for structures subjected to bending. In the same manner, type C3D10 identifies a 3-dimensional continuum element with 10 nodes and enables the users to mesh complex geometries more conveniently as compared to elements

type C3D8 resp. C3D8I. The element types C3D8I and C3D10 were used in this study to model the brake components. Detailed information about the other types of elements can be found in the Abaqus documentation [Aba14].

The definition of a contact pair in Abaqus requires one master and one slave surface. The two types of the contact discretization in Abaqus are “node-to-surface” and “surface-to-surface”. In node-to-surface discretization, a slave node has an interaction with a group of master nodes and is not allowed to permeate the master surface. However, the nodes of the master surface can penetrate the slave surface. In contrast to node-to-surface, contact conditions in surface-to-surface are evaluated not only at a single slave node but also at the region around this slave node. Therefore, the accuracy of the contact pressure is higher in surface-to-surface discretization

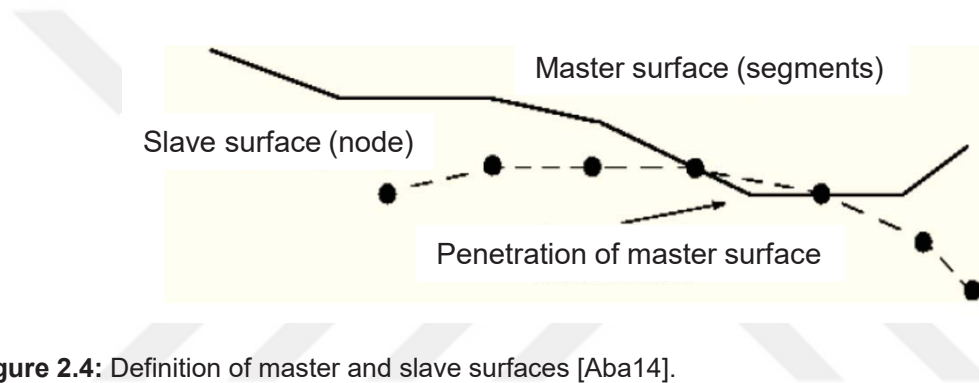


Figure 2.4: Definition of master and slave surfaces [Aba14].

In order to extract the natural frequencies and mode shapes of each brake component, a Normal Modal Analysis (NMA) is performed [Bak05]. The natural frequencies and mode shapes obtained via NMA are compared with the experimental results. Subsequently the model updating technique is applied by tuning material properties, such as Young’s modulus, density and Poisson’s ratio [Bak05].

The equations of the motion for a structure can be written as follows [Bak05]:

$$[M](\ddot{x}) + [C](\dot{x}) + [K](x) = (F) \quad (2.2)$$

where $[M]$ is the mass matrix, $[C]$ is the damping matrix and $[K]$ is the stiffness matrix. The vectors (\ddot{x}) , (\dot{x}) and (x) denote acceleration, velocity and displacement respectively. The vector, (F) represents the externally applied load on the system.

In case a structure is vibrating freely while there is no external load and damping effect, the Equation 2.2 is simplified as [Bak05]:

$$[M](\ddot{x}) + [K](x) = 0 \quad (2.3)$$

To calculate the natural frequencies of a structure, assuming a sinusoidal motion $((x_i) = (u_i)e^{j\omega t})$, Equation 2.3 can be rewritten as a real eigenvalue problem [Bak05]:

$$([K] - \omega_i^2[M])(u_i) = 0 \quad (2.4)$$

where ω_i denotes the natural frequency at the i^{th} mode of the structure and the u stands for the associated mode shape.

The equations of motion for a system, which has no external load and is self-excited, can be written as [Bak05]:

$$[M](\ddot{x}) + [C](\dot{x}) + [K](x) = 0 \quad (2.5)$$

After the eigenvalue problem is solved, the eigenvalues are derived as a complex number $\lambda_i = \alpha_i + i\omega_i$ where α_i and ω_i represent the real and imaginary part of the i^{th} mode.

2.1.3 Instability Analysis of the Brake System via CEA

The eigenvalue problem for the brake system can be written as follows [Bak05]:

$$([K_T] + \omega_i[C] - \omega_i^2[M])(u_i) = 0 \quad (2.6)$$

where $[K_T]$ stands for the stiffness matrix, which is unsymmetrical due to the friction. Prior to the CEA of the brake system, a NMA is conducted by omitting the damping matrix and the unsymmetrical friction stiffness matrix to obtain the projection subspace which is necessary to linearize the system. The initial matrixes in Equation (2.6) are projected on the subspace as follows [Bak05]:

$$[M]^* = [u_1, u_2, u_3 \dots u_n]^T [M] [u_1, u_2, u_3 \dots u_n] \quad (2.7)$$

$$[C]^* = [u_1, u_2, u_3 \dots u_n]^T [C] [u_1, u_2, u_3 \dots u_n] \quad (2.8)$$

$$[K_T]^* = [u_1, u_2, u_3 \dots u_n]^T [K_T] [u_1, u_2, u_3 \dots u_n] \quad (2.9)$$

The linearized system can now be expressed as follows [Bak05]:

$$([K_T]^* + \omega_i[C]^* - \omega_i^2[M]^*)(u_i)^* = 0 \quad (2.10)$$

The complex eigenvalues are calculated and obtained as $\lambda_i = \alpha_i + i\omega_i$. The real part represents the decay or growth rate of the oscillation and imaginary part denotes the frequency of the oscillation. If the real part is positive, the system is instable at the corresponding natural frequency [Bak05].

2.2 Analytical Investigations

Diverse analytical approaches have been utilized by scientists to describe the fundamental physical phenomena inducing squeal. The analytical models have low degrees of freedom, which enables fast approximations of squeal propensities. Three squeal mechanisms generally

discussed in the literature are explained in this study. Detailed descriptions of the other mechanisms can be found in the reviews published by Kinkaid et al. [Kin03] and Ibrahim [Ibr94].

2.2.1 Stick Slip

As cited by Kinkaid et al. [Kin03], Mill [Mil38] purposed the reason of squeal as a negative friction-velocity slope, which is mathematically defined as $\partial\mu_d/\partial v < 0$. Kinkaid et al. [Kin03] explained this mechanism with the aid of an oscillator model, shown in Figure 2.5. At a point in time the condition $\mu_s > \mu_d$ is fulfilled. The mass sticks to the sliding surface so no relative movement is observed. As the mass moves along the x-direction, the spring force increases. At a certain point it becomes higher than the friction force. Hence the mass starts to slip, moves in negative x-direction and the tension in the spring is relieved ($\mu_s < \mu_d$). This behavior repeats itself, which is regarded as a self-excited oscillation [Kin03].

The governing equation of the oscillator depicted in Figure 2.5 is written as follows [Kin03]:

$$m\ddot{x} + (c - mg\mu_b)\dot{x} + kx = 0 \quad (2.11)$$

where x denotes the displacement and m stands for the mass of the block. The relationship between dynamic coefficient of friction, μ_d , at a velocity, v , is defined as [Kin03]:

$$\mu_d = \mu_a - \mu_b v \quad (2.12)$$

where μ_b and μ_a are constants. If the condition $\mu_b > c/mg$ is fulfilled, a negative damping effect occurs and the system becomes unstable. Based on this derivation Fosberry and Holubecki [Fos61] stated that friction induced vibrations can be the result of a system possessing a higher static friction coefficient than dynamic friction coefficient or whose dynamic friction coefficient decreases as velocity increases.

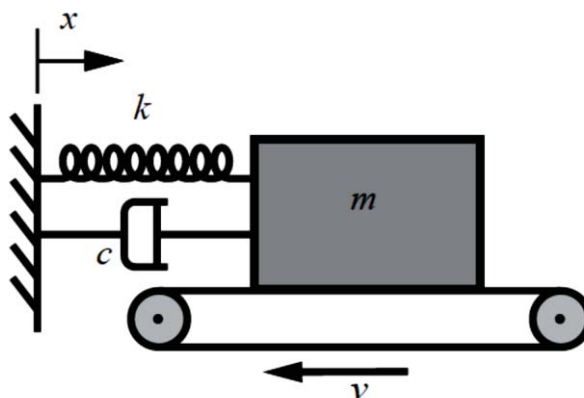


Figure 2.5: Schematic of a spring-mass-damper system on a sliding surface [Kin03].

2.2.2 Sprag Slip

As reported by Kind et al. [Kin03], Spurr [Spu61] proposed a model for a squeal mechanism. According to the author, the reason for squeal occurrence is a consequence of the geometric coupling. Spurr [Spu61] performed experiments with the chamfered brake pads and the rotor as illustrated in Figure 2.6. The test setup is shown as simplified model consisting of a rigid rod and a moving rigid plane in Figure 2.6b.

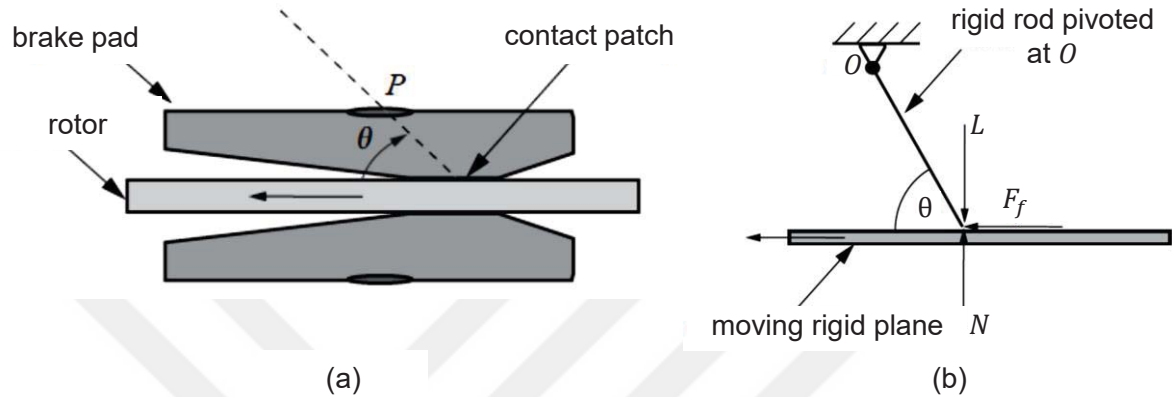


Figure 2.6: a) Spurr's test setup for sprag slip a) The simplified model of Spurr's test setup, adapted from [Kin03].

Spurr expressed the equilibrium condition for this system as [Spu61]:

$$N = \frac{L}{1 - \mu \tan \theta} \quad \text{and} \quad F_f = \frac{\mu L}{1 - \mu \tan \theta} \quad (2.13)$$

where N is the normal load, F_f is the friction force, μ is the coefficient of friction and θ denotes the angle between the rigid rod and the moving rigid plane. In case θ approaches to $\arctan(1/\mu)$, the value of the normal load N tends to infinity. Hence, the rotor and pads are coupled and they move together, which was dubbed “spragging” by Spurr [Spu61]. The coupled movement continues until the coupled components are deformed adequately because of the high normal forces and friction forces in contact [Kin03]. The flexibility of the pads and rotor releases the rotor to move individually. With an assumption for a constant rotational speed of the rotor, the spragging and releasing conditions occur in cycles, which is regarded as a “sprag-slip” mechanism [Kin03].

The “sprag-slip” mechanism was later investigated by Jarvis and Mills [Jar63] who utilized an enhanced version of Spurr's model [Kin03]. They employed the model of a cantilever beam on a disc to study the mechanism (Figure 2.7). The main conclusion of their work is, that the instability of the system is observed as a consequence of the geometric coupling of the components. Hence, they championed the Spurr's work [Kin03]. They also added that the instability detected in their system was not related to variations of friction as a function of velocity.

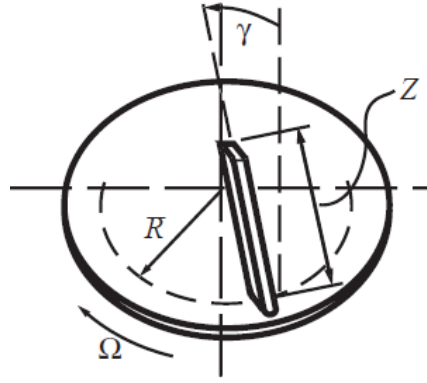


Figure 2.7: The model of Jarvis and Mills [Jar63]

2.2.3 Mode Coupling

As stated by Nobari [Nob15], North [Nor72] proposed that an asymmetric stiffness matrix, which occurs because of friction, in a lumped-mass model results in brake squeal. This mechanism was investigated by Hoffmann et al. [Hof02] by employing a system with two degrees of freedom (Figure 2.8). As stated by Nobari [Nob15] the equation of motion for Hoffman's model can be derived as follows [Nob15]:

$$\begin{bmatrix} m & 0 \\ 0 & m \end{bmatrix} \begin{pmatrix} \ddot{x} \\ \ddot{y} \end{pmatrix} + \begin{bmatrix} k_{11} & k_{12} \\ k_{21} & k_{22} \end{bmatrix} \begin{pmatrix} x \\ y \end{pmatrix} = 0 \quad (2.14)$$

where the components of the stiffness matrix are obtained as:

$$k_{11} = k_1 \cos^2 \alpha_1 + k_2 \cos^2 \alpha_2 \quad (2.15)$$

$$k_{12} = k_1 \sin \alpha_1 \cos \alpha_1 + k_2 \sin \alpha_2 \cos \alpha_2 - \mu k_3 \quad (2.16)$$

$$k_{21} = k_1 \sin \alpha_1 \cos \alpha_1 + k_2 \sin \alpha_2 \cos \alpha_2 \quad (2.17)$$

$$k_{22} = k_1 \sin^2 \alpha_1 + k_2 \sin^2 \alpha_2 + k_3 \quad (2.18)$$

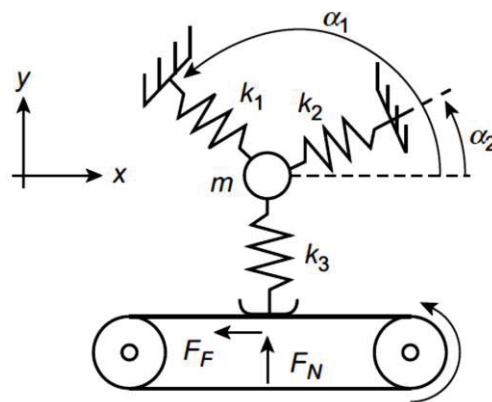


Figure 2.8: System studied by Hoffmann et. al [Kin03]

In order to explain the effect of the friction coefficient on squeal according to the model of Hoffmann et al., Nobari [Nob15] performed a CEA on Hoffmann's model and calculated the eigenvalues of the system as $\lambda_{1,2} = \pm[-2 \pm \sqrt{1 - 4\mu/3}]^{1/2}$. He identified three different conditions plotted the results regarding the change in natural frequencies and eigenvalues as a function of the friction coefficient μ (Figure 2.9). If $\mu < 0.75$ (Zone 1), both eigenvalues are imaginary and their values converge as the coefficient of friction approximates to 0.75. In case of $\mu = 0.75$, the eigenvalues are identical and are pure imaginary numbers. If $\mu > 0.75$ (Zone 2), the real parts of the eigenvalues are different from 0 and their algebraic signs are different whilst the values of the imaginary parts of both eigenvalues remain the same. A positive real part results in a negative damping of the system and leads to instability. Therefore, this mechanism is regarded as mode coupling.

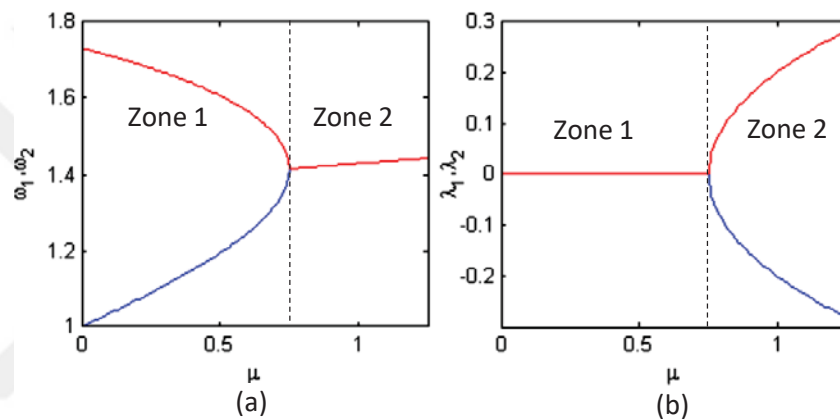


Figure 2.9: According to the Hoffman's model, changes in (a) natural frequencies and (b) real parts, adapted from [Nob15].

2.3 Experimental Investigations

Fieldhouse and Newcomb [Fie93] investigated squeal by utilizing holographic interferometry technique. They pointed out that the measured squeal frequencies were close to the natural frequencies of the brake components. They presumed that adjacent natural frequencies are coupled by friction. Moreover, the authors claimed, that the excitation of the brake pads has a great influence on squeal. They also highlighted that the brake disc is in bending mode at squeal events and the system becomes instable most possibly as a consequence of vibrations of the brake pad.

Ishihara et al. [Ish96] studied on the dynamic behavior of the caliper by employing accelerometers. At a predetermined rotational speed and brake pressure, they applied random excitations to the caliper by utilizing an electromagnetic shaker. The authors stated, that the mode shape of the caliper in its diagonal direction and the stiffness of the friction material in its out of plane direction have a big contribution in squeal. They showed that the squeal

frequency raised as applied pressure is increased. Suggestions given for squeal treatment were modifications of the stiffness of the friction material and a reduction the coefficient of friction between the friction material and the brake disc. In addition, they purposed that changing material of the disc and its geometry might be a treatment to deal with squeal.

Reves et al. [Ree00] utilized high speed electronic speckle pattern interferometry (ESPI) to investigate the out of mode shapes of the brake disc whilst the brake system squeals. A complex mode is created by means of the superposition of two diametric modes which are of the same order and displayed a difference in phase. They pointed out that this mode may be an excitation mechanism for high frequency brake noise.

Kummamoto et al [Kum04] worked on the correlation between the contact conditions of pad/caliper and the initiation of squeal. They placed an accelerometer on the caliper to measure the vibration and employed pressure sensors to monitor the contact distribution between caliper and brake pad. They detected two squeal frequencies as a consequence of the pads' irregular movement in their tangential direction. They pointed out that the disturbed movement of the pads was a result of a light contact of the brake pad and the caliper. They concluded that a rigid connection between the pad and caliper might be a treatment for squeal.

2.4 Finite Element Approach

Liles [Lil89] was the first author who employed finite element analysis for the investigation of brake squeal. He performed a CEA for his brake model, which involved pad, disc, and caliper, in order to determine designs which are less prone to squeal. The author claimed that the squeal can be diminished by using stiffer friction material whose width is also short. On top of that, he stated that using a relatively softer disc can be the solution to reduce squeal propensity. He also mentioned that a higher coefficient of friction can increase the squeal propensity as stated by Ishihara et al. [Ish96].

Bajer et al. [Baj04] studied on damping effects caused by friction to improve over-under estimations in CEA. They concluded that the negative damping effect caused by the friction coefficient which is the function of the velocity. This is the reason of overestimations of the number of unstable modes in brake model. The positive damping, which occurs in the contact due to the friction, has positive effect to eliminate the overestimations.

Junior et al. [Jun08] investigated the influence of the operational parameters on the stability of a brake system. They mentioned, that an increase in temperature decreases the stiffness of the pad, hence the coupling mechanism changes between the pad and disc. Moreover, an increase in the coefficient of friction increases the instability of the brake system. These findings meet with the results obtained by with Liles [Lil89] and Ishihara et al [Ish96]. In addition,

the authors stated, that the power balance method is beneficial as compared to other methods to validate the contact stiffness between the brake pad and the brake disc.

Bakar [Bak05] validated his brake model by means of the modal analysis and contact analysis. The modal properties of the components were validated by FE model updating. The validation of the contact analysis between pad and disc was performed in terms of pressure distribution. He also took the real surface topology of the pad into account in his CEA to improve the predictions for the dynamic instabilities of the brake system. He stated that the results of the pad with real surface topology in simulation is well correlated with experiment results in terms of pressure distribution on the pad surface.

2.5 Treatments for Disc Brake Squeal

Liu and Pfeifer [Liu00] studied on the suppression of brake squeal via geometrical modifications of the brake pad. Their model included only the pads and the disc, which allowed them to evaluate the analyses quickly and to simulate a high number of design variants. They stated that the chamfers and slots applied on the pads are effective solutions for squeal at some frequencies. However, they observed that these modifications can cause an increase in noise at other squeal frequencies.

Cunefare and Graf [Cun02] presented a method based on the 'dither' control to suppress squeal. The dither control provides a frequency which is relatively higher than the squeal frequency so that squeal in the brake system can be eliminated via utilization of the harmonic forces of a frequency which is higher than the squeal frequency. A stack of piezoelectric elements was mounted in each piston to generate harmonic force. Furthermore, they stated that the squeal can be even prevented by utilization of this method, before squeal occurs.

Chen [Che09] presented a guideline on methods frequently utilized in the automobile industry. The first one, which is economically inefficient, is to obtain a friction material which is not prone to squeal by alteration of its constituents. The second method includes, changing mass and stiffness of the components whose modes are merging. According to the third method, chamfer can be applied on the friction material, which changes the modal characteristic of the pad. Finally, a proper selection of the shim can damp the excitations and adjust the pressure distribution. The author also added that modifications on the location and shape of the fingers of the caliper can be a treatment for squeal as well.

Massi and Giannini [Mas08] studied the influence of the modal damping on squeal propensity by working on a beam-on-disc setup. They applied worked on different structural damping scenarios by applying structural damping beam and disc. They stated that two important effects were observed. Firstly, an homogenous increase in structural damping results in an increase in modal damping of the merging modes. Secondly, a nonhomogeneous increase in system

damping causes a difference in damping between the merging modes, which increase the squeal propensity of the brake system.

3 Experimental Modal Analysis

3.1 Introduction

3.2 Experimental Setup

In this study, the experimental modal tests were conducted by using a Brüel & Kjaer (B&K) data acquisition system. Firstly, modal testing for the single brake components, which are brake disc, brake pad, caliper and carrier, were performed. The test were executed under a so called free-free boundary condition, which can be hypothesized as a structure which moves freely in the air without any boundary constraint. Modal testing under this boundary condition enables to extract the pure dynamic behavior of a structure. In case of other boundary conditions, which greatly limit the degrees of freedom, e.g. joining by welding or clamping, the stiffness matrix of a structure might be influenced and modal testing results could be over-/underestimated. Hence for this study, the brake components were hung on a tripod microphone stand by using fishing line to provide an approximately free-free boundary condition. The test setup for each component is presented in proceeding chapter.

Secondly, modal testing was executed for the brake assembly under a brake line pressure of 2 bar, so that a contact between brake pad and brake disc is ensured. The nonlinear material behavior of the friction material, varying pretension of the bolts, the flux of force in other joining connections, sealing parts at guiding pins and pistons, as well as the brake oil in the caliper have influence on the stiffness of the assembly. Therefore, an extraction of the dynamic behavior for the whole assembly can only be challenging. In the scope of this study, modal testing of the brake assembly was conducted by using the measurement points used for the modal testing of the brake disc.

The required number of excited and measured nodes depends on the complexity of a structure. Only with sufficient number of nodes, the mode shapes of a structure can be illustrated precisely. Furthermore, the location of the measurement points on the structure is important to distinguish the different mode shapes adequately. To define the number of measurement points and their location on a structure, the mode shapes of the components were extracted numerically. In Figure 3.1, two different mode shapes of the brake disc are illustrated. The mobility of the points on the disc at a corresponding frequency is classified with different colors. To make it convenient to define moving and not moving points, they are called antinode and

node respectively. The required mode shapes of a structure at a frequency of interest should be taken into account before the number of measurement points and their locations are defined. For instance, selecting just a few mode shapes at either low frequencies or high frequencies might result in missing information of nodes and antinodes in the experimental FRF measurements. Therefore, some of the mode shapes might not be detected in modal analysis.

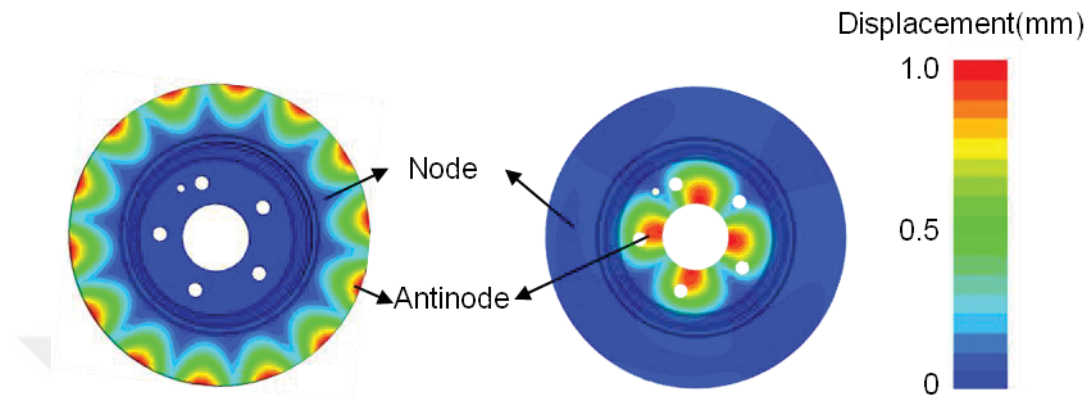


Figure 3.1: The nodes and antinodes on two different mode shapes of the disc

In modal testing of the components and the assembly, B&K 4508 type uniaxial accelerometer was attached on the measurement points by using beeswax. B&K 8206 type hammer with steel tip was used for the excitation of the components. In order to conduct the modal testing, the rowing hammer technique was utilized to extract the FRFs [Ewi00]. In this technique, the accelerometers are permanently attached at selected measurement points while the remaining points are successively struck with the hammer (Figure 3.2). The mounted four accelerometers at the measurement points 3, 6, 10, 15 on the brake disc are shown in Figure 3.2.

The acquired input and output analog signals by modal testing are processed in DAQ. In the configuration section of the analyzing software, the frequency span was set between 0 Hz and 12,800 Hz. The number of spectral lines was selected as 6,400 which equals to a 2 Hz frequency resolution in the FFT analysis. The Uniform Window, which is regarded as unity gain weighting function [Avi14], was used for both excitation and response signals in FFT process.

For each brake component, the mode shapes on corresponding frequencies were drawn by gathering the FRFs of the structure. The mode shapes of the components were plotted by means of self-written Matlab scripts, using the quadrature-picking technique, which utilizes the imaginary part of the frequency response function [Døs88]. The experimentally extracted mode shapes of the components are illustrated in Chapter 4 to compare them with the equivalent mode shapes obtained numerically.

3.3 Modal Testing of Disc Brake Components

3.3.1 Brake Disc

Figure 3.2.a illustrates the experimental setup for the brake disc. The material of the brake disc is cast gray iron GG20. For the modal testing of the disc, 16 measurement points on the friction ring (1-16) and 9 additional measurement points on the top hat section of the disc (17-25) were marked (Figure 3.2.b). Four accelerometers were used to collect the response signal for each FRF measurement. In case a accelerometer placement on one of the node of the disc, more than one accelerometer were used. In total 25 FRFs were obtained for the brake disc by applying excitation in out of plane direction of the disc.

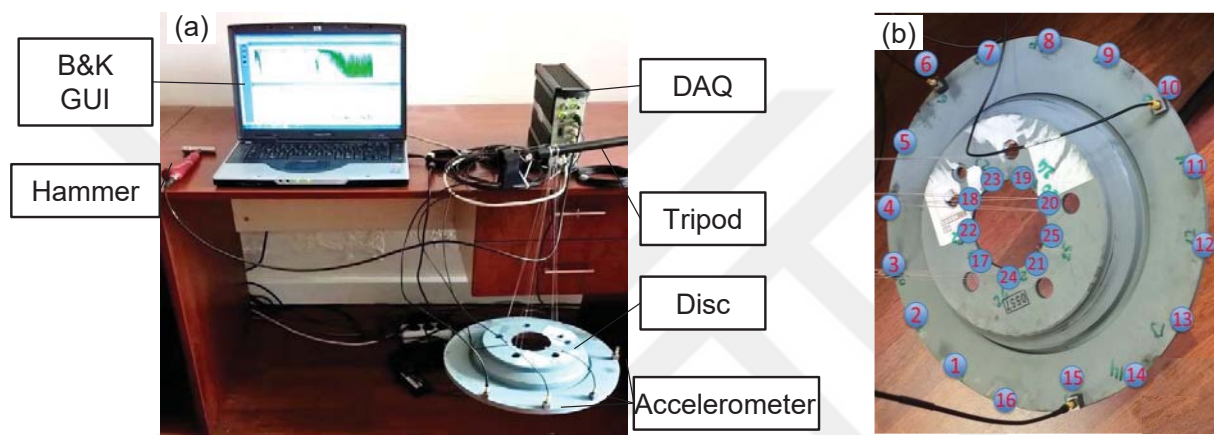
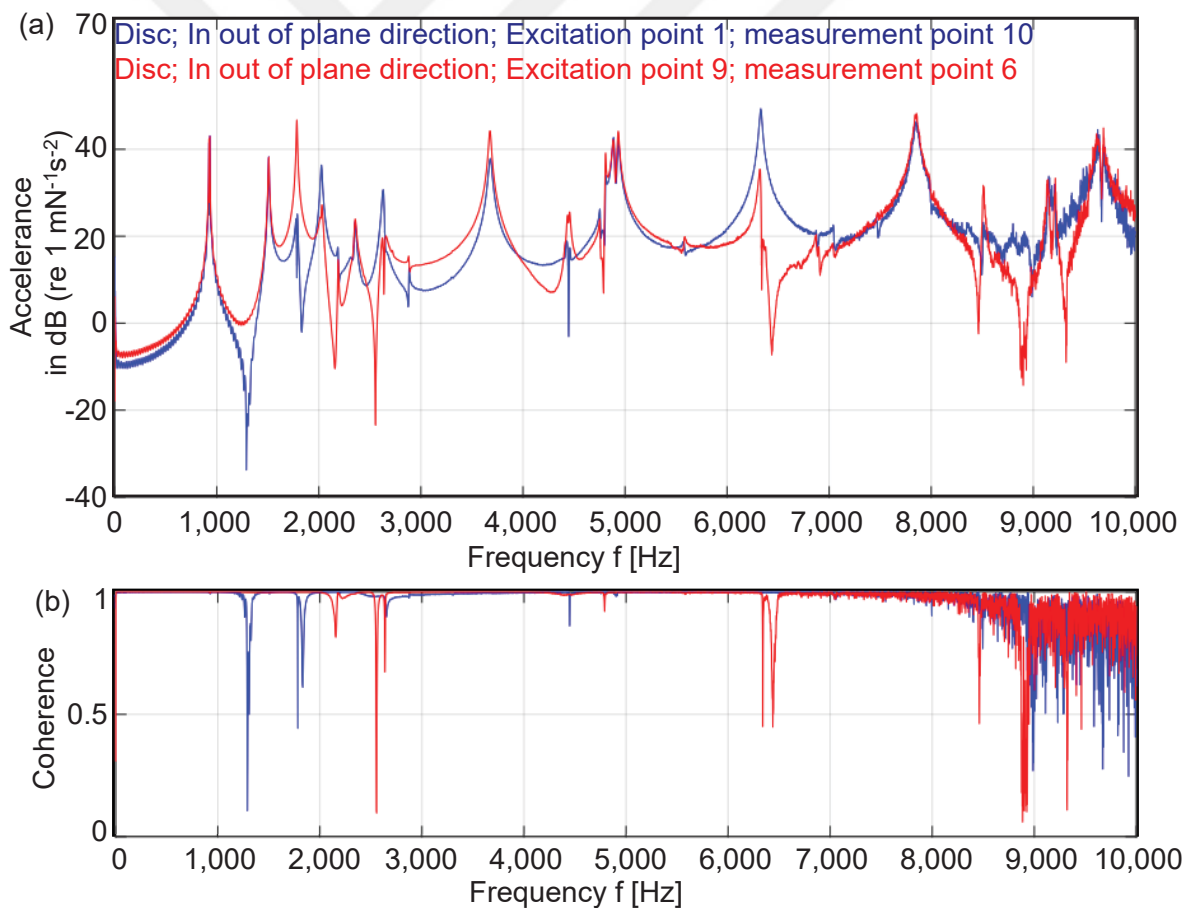


Figure 3.2: a) The experimental setup for the disc b) The measurement points on the disc

As example of a modal testing on the brake disc two FRF measurements are illustrated in Figure 3.3.a. In the first measurement, excitation point is 1 and the response is collected by an accelerometer placed on point 10. In second measurement, excitation point 9 and the response is measured at point 6. Both measurements show the same values of the natural frequencies for corresponding modes (Figure 3.3.a). It can be clearly seen that the peaks in FRF at the natural frequencies are very sharp, which shows that the material damping of the disc is very small at these particular frequencies. The coherence function versus frequency domain is illustrated in Figure 3.3.b. A good coherence is achieved up to 8,000 Hz, which means that the FRF measurement is reliable up to this frequency. The measured natural frequencies with the associated modes are given in Table 3.1.

Table 3.1: The natural frequencies for the modes of the disc

Mode No.	Frequency [Hz]	Mode No.	Frequency [Hz]
1	932	6	2,630
2	1,510	7	3,676
3	1,784	8	4,934
4	2,026	9	6,330
5	2,356	10	7,856

**Figure 3.3:** The results of two modal testing on the disc with a) FRFs b) Coherence functions

3.3.2 Brake Pad

The brake pad was hanged to the tripod as illustrated in Figure 3.4. The brake pad consists of a friction material, a back plate and a shim (Figure 3.5.a). The back plate is made of steel. The friction materials contain nonferrous metals, inorganic and organic fibers, abrasives, lubricants and property modifiers such as glass, rubber, and carbon. In addition, the material has an anisotropic and non-homogeneous characteristic. Moreover, a shim is used to prevent brake squeal and therefore has a damping effect on the structure due to its multilayer composition. Within the scope of this study, the shim was removed from the back plate to reduce the complexity of the structure before modal testing was performed. The excitation points were marked on the back plate by means of a pre-simulated modal analysis of the brake pad (Figure 3.5.b). The accelerometer was attached on point 1 and the brake pad was excited on all points in z direction.

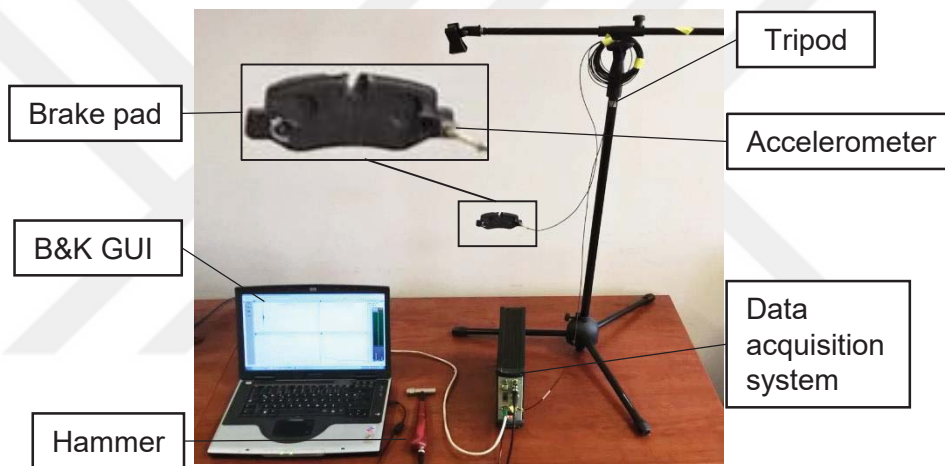


Figure 3.4: The experimental setup for the brake pad

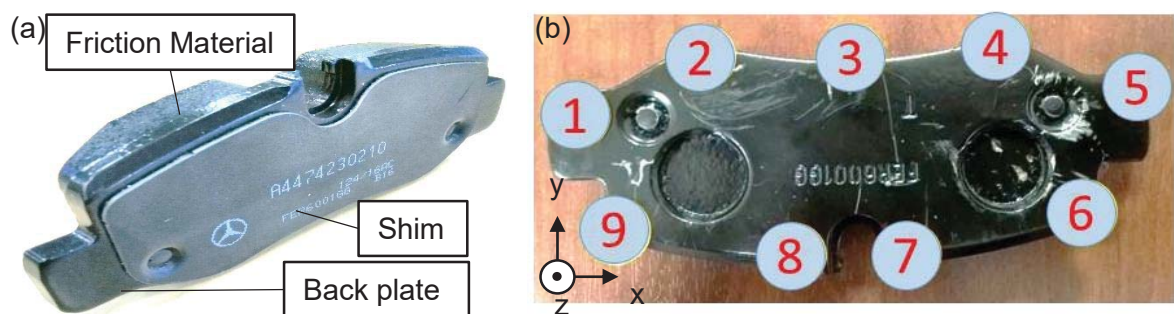


Figure 3.5: a) The brake pad and b) The measurement points on the back plate

Figure 3.6 shows two FRFs and the corresponding coherence functions of impact tests on brake pad, when the accelerometer was mounted at point 1 and the excitation was performed on reverse side of point 1 and point 5 in +z direction. The first three natural frequencies of the brake pad are 3,720 Hz, 5,590 Hz and 7,780 Hz. Due to the excessive damping in the non-homogenous friction material, the coherence level becomes poor after roughly 4,000 Hz.

Although there is a poor coherence value given for the second and third natural frequency, the peaks can be predicted and the quantitative result assumed to be valid.

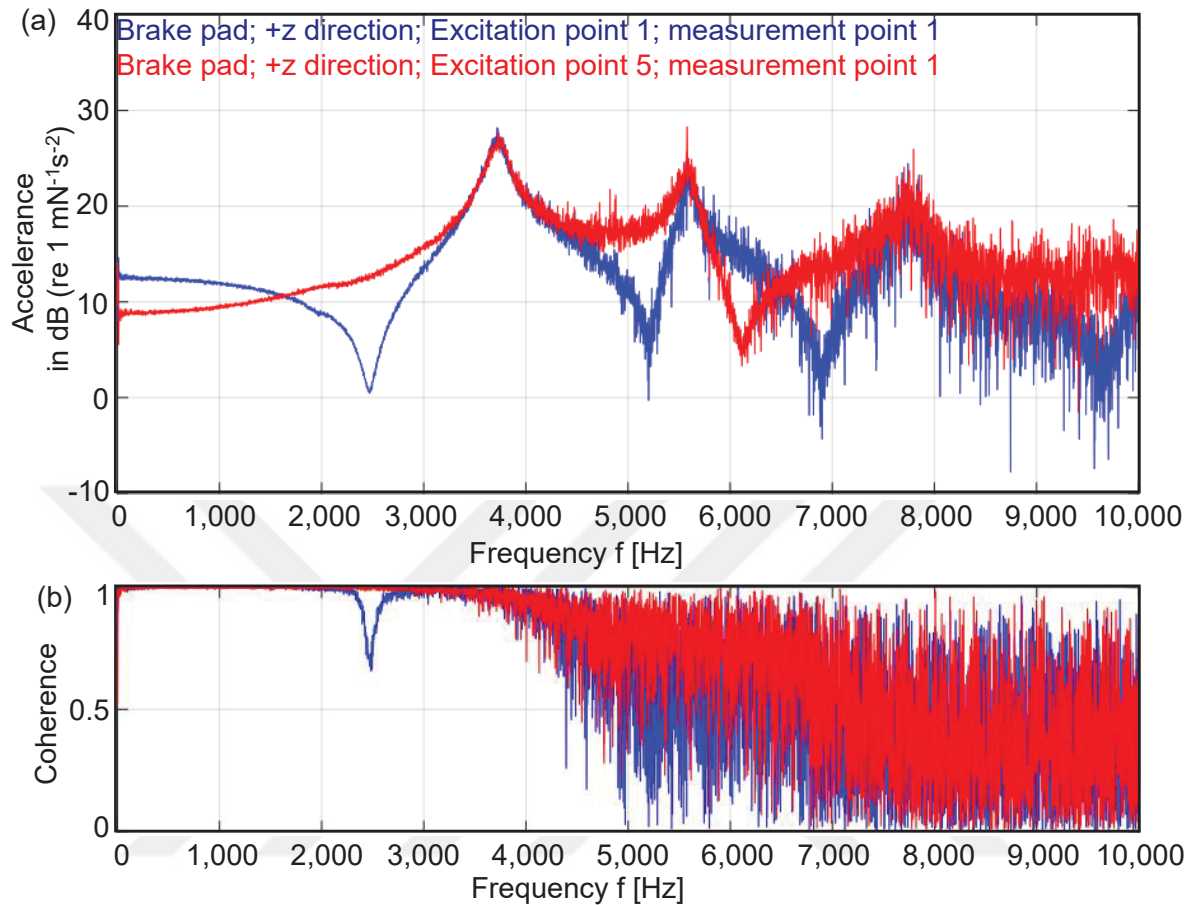


Figure 3.6: The results of two modal testing on the brake pad with a) FRFs b) coherence functions

The effect of production variability on natural frequencies was investigated by performing modal testing on eight brake pads (Figure 3.7). The excitation and response points were the same for every brake pad as depicted in Fig. 3.5.b. Although all the brake pads were provided by the same company, the natural frequencies first two modes of the brake pads spread within a span of ca. 200 Hz and their averaged values are 3,769 Hz and 5,539 Hz. For the third mode of the brake pad, the dispersion of natural frequency is greater than 200 Hz and its average value is 7,433 Hz. The validation of the FE model is executed based on the modal parameters obtained through the experiments. Therefore, the differences in the natural frequencies of the brake pad due to the production variability must be taken into account in the validation stage of the brake pad in FE modelling.

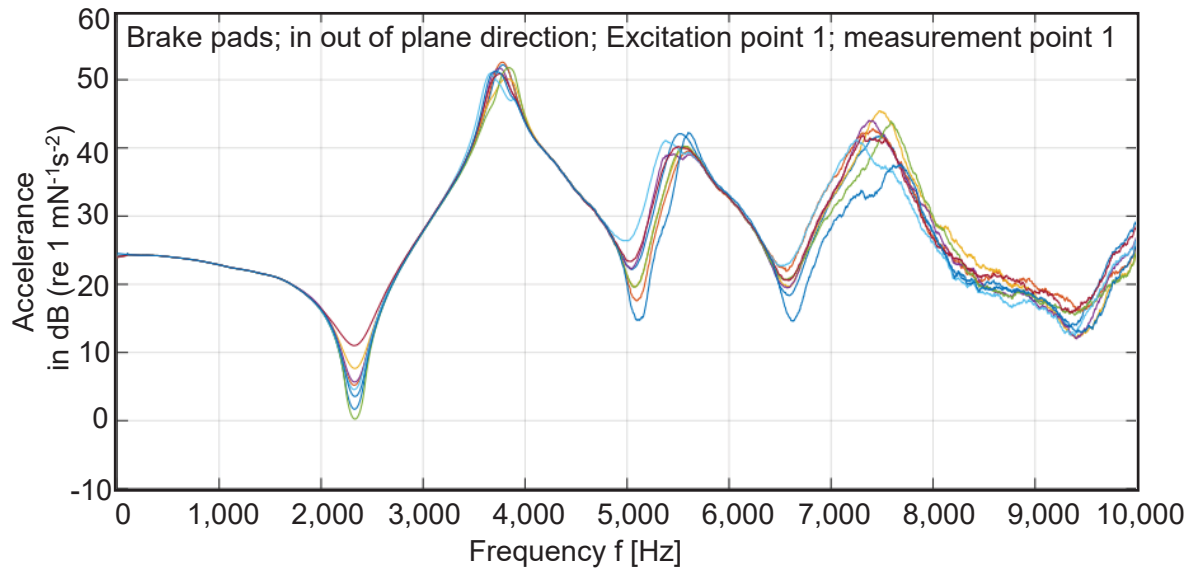


Figure 3.7: The FRFs of eight brake pads.

3.3.3 Carrier

The experimental setup for the carrier is shown in Figure 3.8.a. The excitation points on the carrier were marked as depicted in Figure 3.8.b and the modal testing was conducted in three directions for each point. Due to the geometric restrictions at point 6 and point 1, the impact tests could only be performed in z and y direction. Three accelerometers were mounted at points 3, 5 and 2. In total, 28 successful modal tests were conducted and 8 modes of the carrier were derived. Table 3.2 shows the natural frequencies of the carrier.

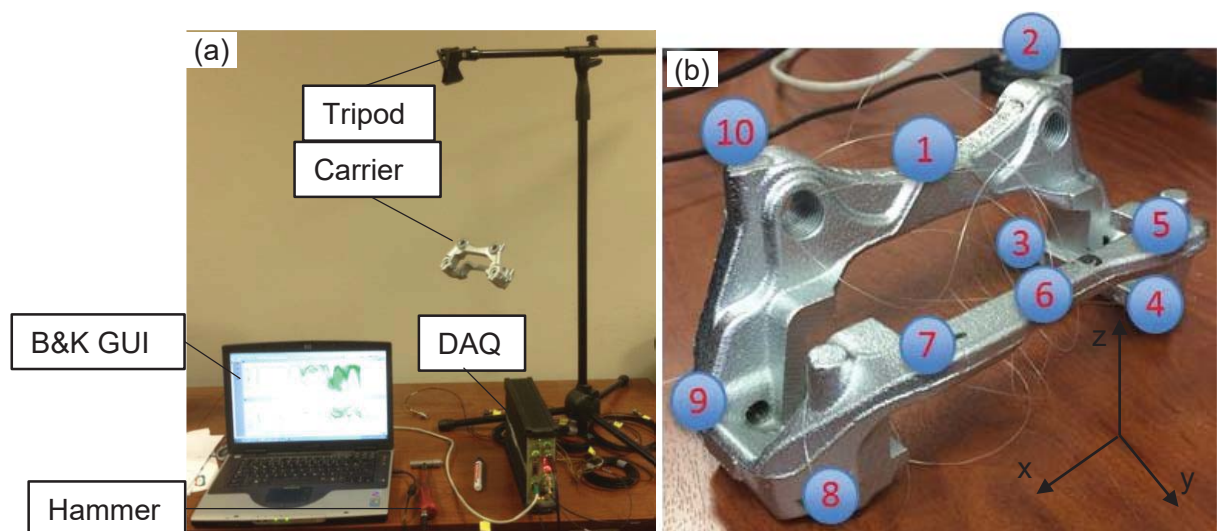


Figure 3.8: a) The experimental setup for the carrier b) The measurement points on the carrier

Table 3.2: The natural frequencies for the modes of the carrier

Mode No.	Frequency [Hz]	Mode No.	Frequency [Hz]
1	1,008	5	3,480
2	1,654	6	5,720
3	2,626	7	5,950
4	2,900	8	6,846

Figure 3.9 shows the two modal testing results derived on the carrier. The FRFs and the coherence functions of the carrier were obtained by applying excitations at point 9 and 3 in +x direction while the responses were measured at point 3 in +x direction. The coherence function of the impact testing on the caliper indicates a good linearity up to 7,500 Hz. Below this value, sudden drops in the coherence function are observed at certain frequencies. As was discussed in theory this is due to the fact that the FRF has a low amplitude at anti-resonances and the coherence value is close to zero. However, these poor values at anti-resonance are acceptable as stated by Avitable [Avi14].

3.3.1 Caliper

The experimental setup for the caliper is illustrated in Figure 3.10.a. The measurement points on the caliper were marked according to Figure 3.10.b and four accelerometers were mounted at point 3 in +z direction, point 2 in +y direction, point 8 in +z direction and point 13 in +x direction (Figure 3.11.b). Impact hammer tests were executed at all points in applicable directions. Hence, in total, 32 measurements were conducted.

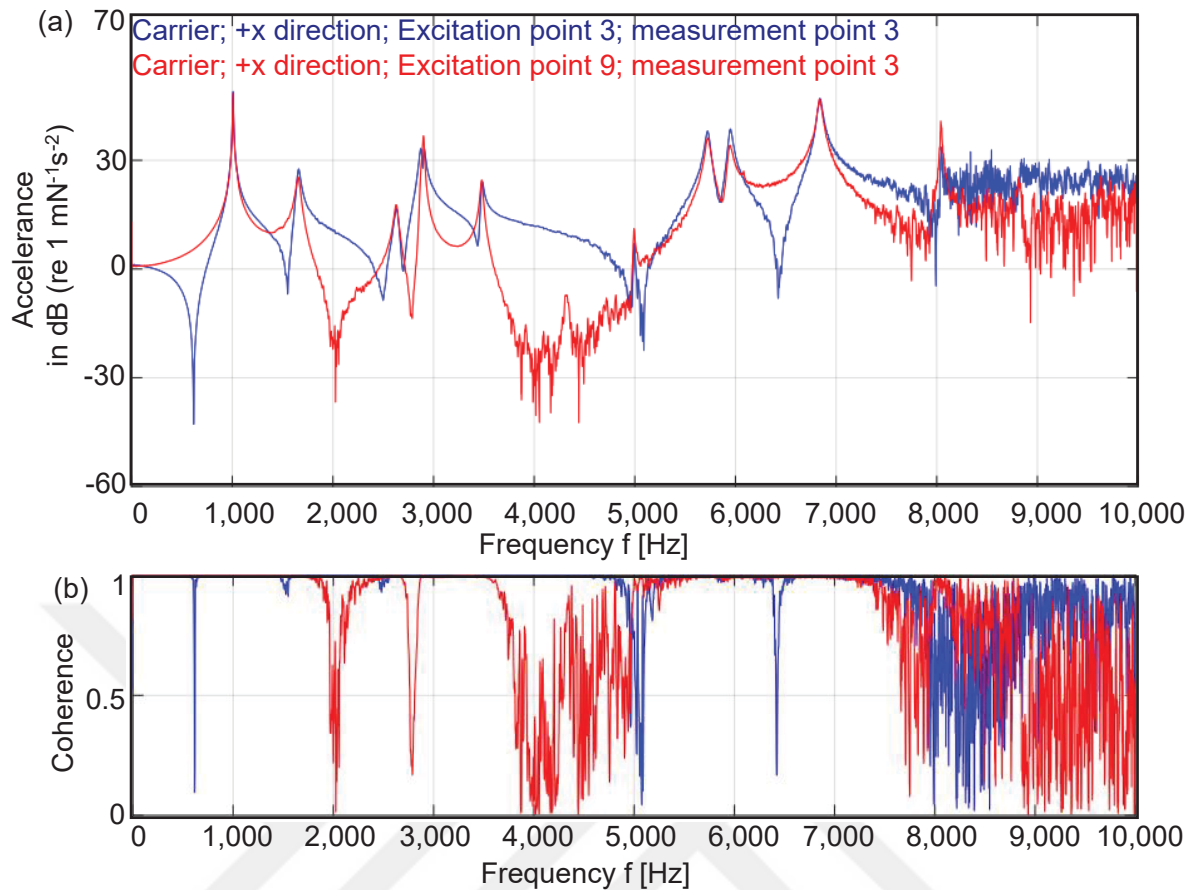


Figure 3.9: The results of two modal testing on the carrier with a) FRFs b) Coherence functions

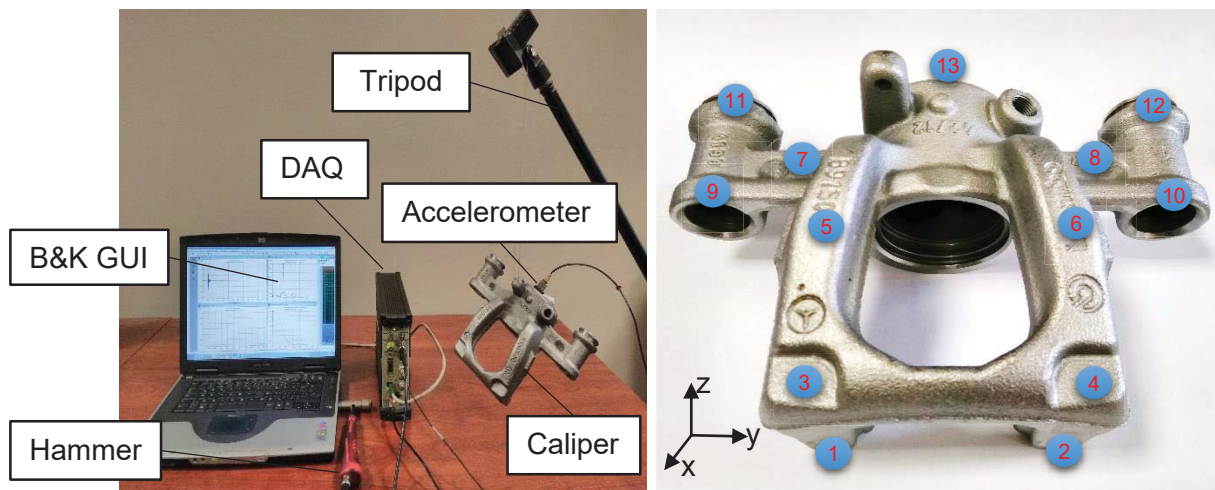


Figure 3.10: a) The experimental setup for the caliper b) The measurement points on the caliper

For two model testing on the carrier the FRFs and coherence functions are shown in Figure 3.11. The natural frequencies at corresponding modes are listed in Table 3.3. The coherence function shows a good linearity up to 6,000 Hz (Figure 3.12.b).

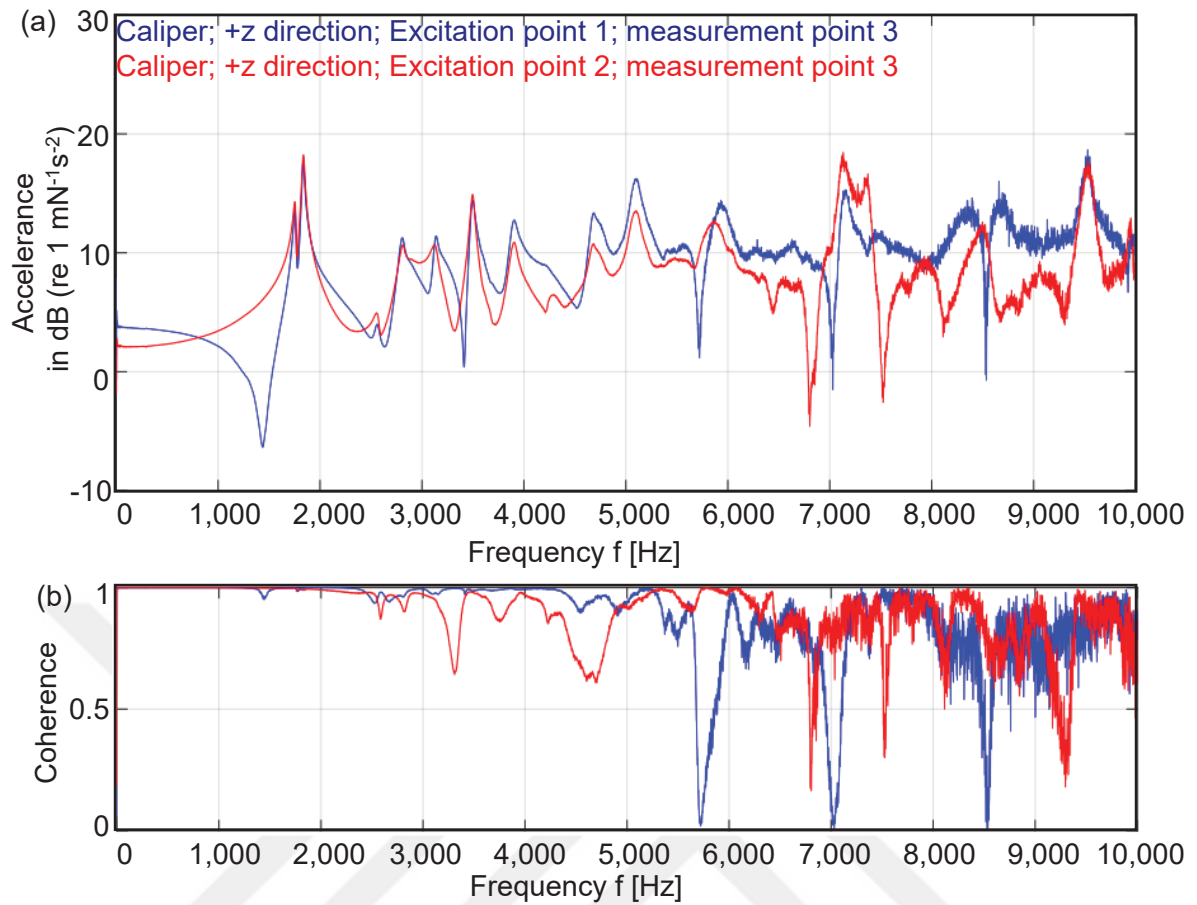


Figure 3.11: The results of two modal testing on the caliper with a) FRFs b) Coherence functions

Table 3.2: The natural frequencies for the modes of the caliper

Mode No.	Frequency [Hz]	Mode No.	Frequency [Hz]
1	1,836	5	3,910
2	2,812	6	4,694
3	3,122	7	5,104
4	3,484	8	5,932

3.4 Modal Testing of Assembly

To extract the natural frequencies of the brake assembly, the modal testing was conducted on the brake disc at the assembled level. The brake line pressure was set to 2 bar (Figure 3.12). This pressure level is the minimum boundary to ensure that the disc does not rotate and has full contact with the brake pads. The number of measurement points and their locations on the brake disc are the same as the ones in the modal testing of the single component (Figure 3.2.b). In modal testing of the brake assembly, the measurement points 6, 7 and 8 had to be skipped due to geometric restrictions of the assembly.

The FRF result of the brake assembly is illustrated in Figure 3.13. The measurement was performed at the driving point 9. The critical natural frequencies of the assembly are 1,816 Hz, 2,686 Hz and 3,630 Hz. In comparison with the FRF result of the free-free conditioned disc, the FRF of the brake assembly shows less number of peaks. Also, these peaks have higher damping than the ones in the FRF of the free-free conditioned disc. The interactions between the disc and the brake pad, the disc and the bolts, as well as the disc and the wheel hub influence the contact conditions in terms of stiffness and damping. Hence, some peaks observed in the FRF of the free-free conditioned disc cannot be detected in the FRF result of the brake assembly.



Figure 3.12: The experimental setup for the brake assembly and the measurement points.

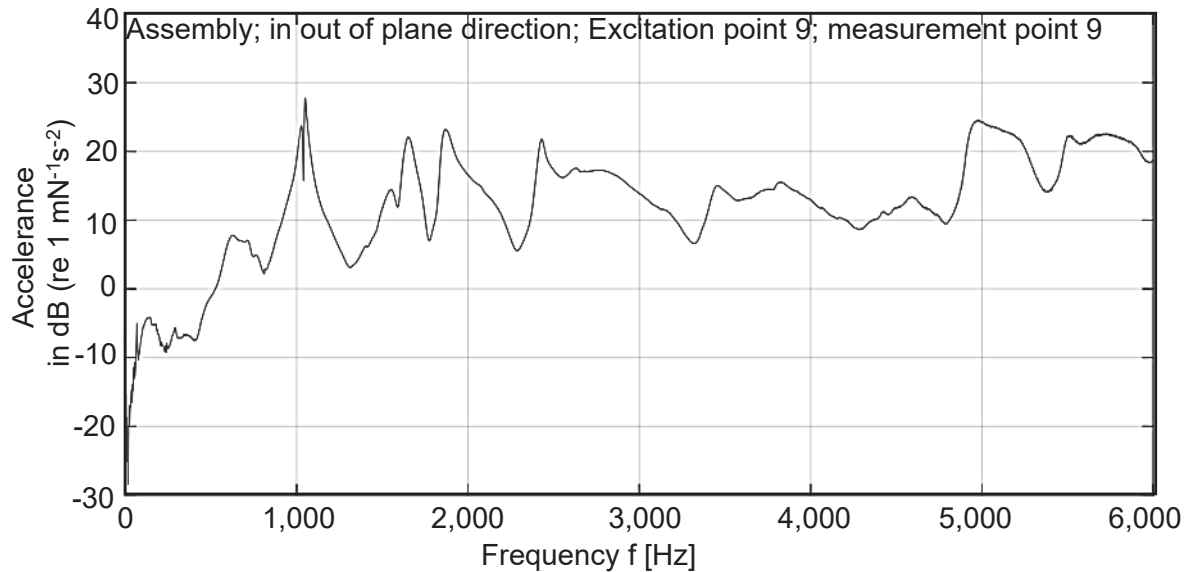


Figure 3.13: FRF of the brake assembly is plotted regarding the driving point 9 and 2 bar brake line pressure

4 Numerical Modal Analysis

4.1 Introduction

The prediction of brake squeal depends on the successful validation of an FE model of the structure investigated, not only at component level but also at assembly level. In this study, the fundamental components as depicted in Figure 4.1 of the brake disc are modeled in Abaqus 6.13. The CAD model of the components are meshed and mesh convergence analysis is conducted. In this chapter, the validation steps for the components as well as for the assembly are addressed. Firstly, the FE models of the components are validated based on the modal parameters as obtained in experimental modal testing i.e. natural frequency and mode shape. Secondly, the validated brake components are integrated in an FE model of the brake assembly. The required contact behaviors are employed in interacting surfaces of the parts. The simulation model is built to include all steps of the braking process, namely applying brake pressure in a static analysis and steady state rotational motion. .

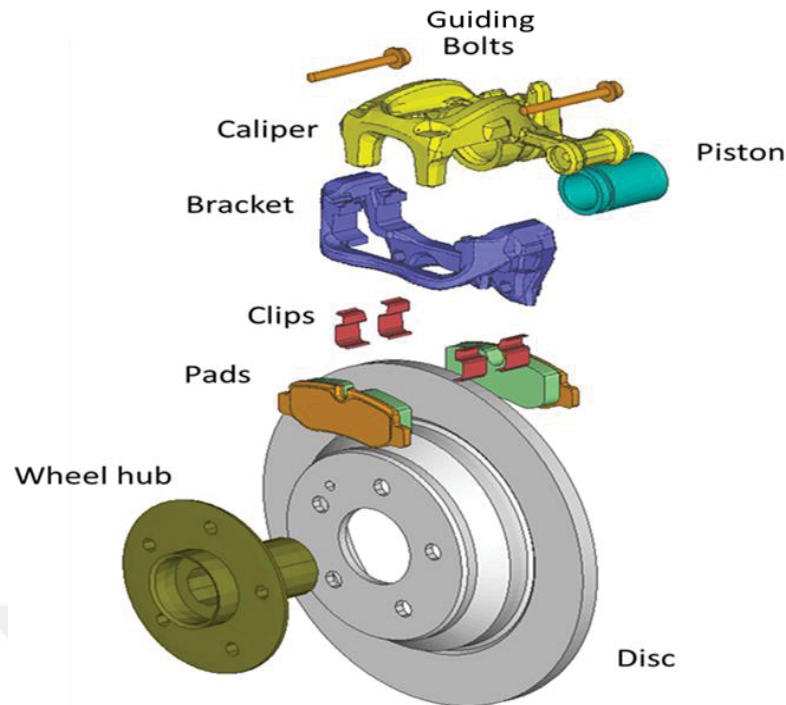


Figure 4.1: The CAD model of the brake disc in this study

4.2 Validation of Disc Brake Components

A mesh sensitivity analysis is performed for each component to select the optimum mesh size which is critical to attain accurate simulation results in a reasonable amount of time. In order to acquire the optimum mesh size for a particular model, a modal analysis is run with two different mesh sizes. The difference in natural frequencies at the same mode is compared for both cases. If the differences are negligible, a coarser mesh size is implemented. If notable differences occur, further mesh refinement and convergence studies are iterated.

The FE models of the components are simulated in free-free boundary condition to match the experimental modal tests. A Lanczos solver is selected for the calculation of the eigenvalues. The calculation provides to evaluate the natural frequencies and associated mode shapes of a component. Based on these two modal parameters of the brake component, the material parameters in the FE model are adjusted within their physical boundaries to match the experimental results. This approach has been used by many authors [Bak05] [Pap07] [Gha11]. Due to the fact that production variability, geometric tolerances and unknown boundary conditions make it difficult to accurately model the behavior of a complex assembly. In this study, FE update is performed as follows: 1) The density of the components are adjusted to their measured mass, after deriving the volume of the components from CAD data; 2) Young's modulus of the material in FE model is tuned to match the natural frequencies attained by modal testing; 3) Poisson ratio is tuned to obtain finer adjustment. In this study, an effect of Poisson ratio on FE update of the components could not be confirmed. Ghazaly [Gha11]

pointed out that the Poisson ratio is recognized to be the least effective parameter to realize a FE update, compared to the density and Young's modulus.. The validation steps of the brake components are illustrated in Figure 4.2.

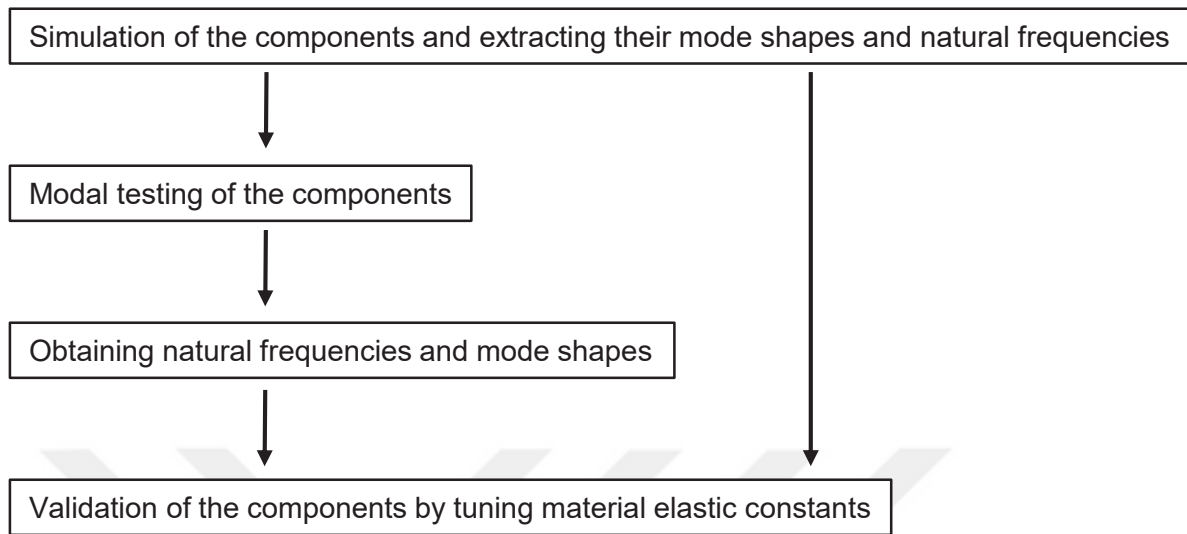


Figure 4.2: The validation steps of the brake components

4.2.1 Brake Disc

The brake disc is modeled with 4,628 hexa elements (type C3D8I) and 7,227 nodes. The results of the numerical as well as the experimental modal analysis are depicted in Figure 4.3 for each natural frequency and corresponding mode shape of the disc. Mode shapes are plotted at corresponding natural frequencies by utilization of self-written Matlab scripts which convert the experimentally obtained FRF of the disc into visual information in which deformed and undeformed shapes are denoted as red and blue wireframes respectively. Not only frequencies but also the mode shapes are well matched by tuning the young modulus of the disc. Except the second and fourth modes of the disc, the relative errors in frequencies are below 5 %.

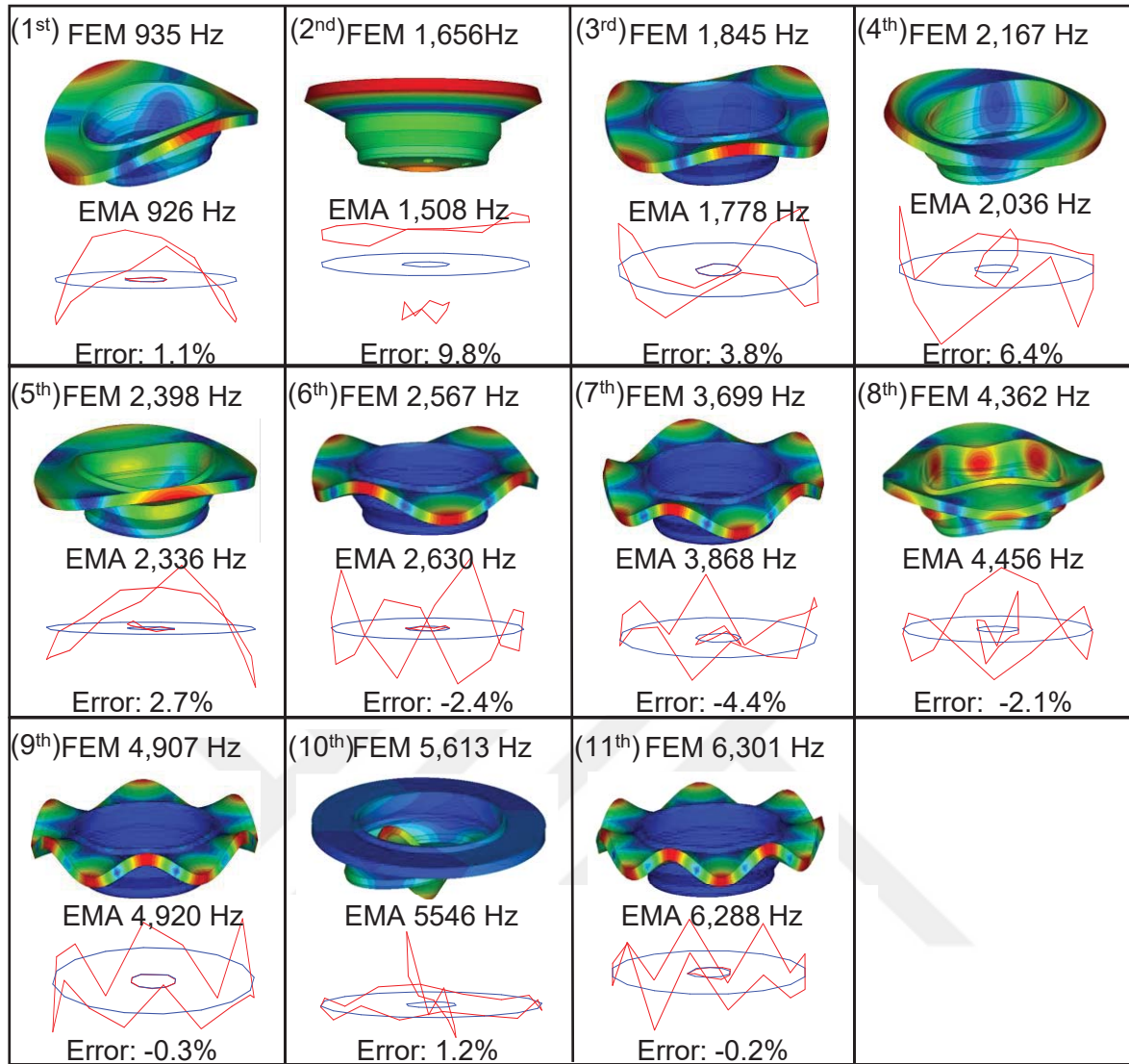


Figure 4.3: The natural frequencies and corresponding mode shapes of the disc

4.2.2 Brake Pad

As illustrated in Figure 4.4.a, the brake pad consists of a friction material and a back plate, which is made of steel. The friction material contains among others nonferrous metals, inorganic and organic fibers, abrasives, lubricants and property modifiers. Hence, the friction material has inhomogeneous and anisotropic characteristics, which results in a nonlinear behavior of the brake pad. As a simplification, transversely isotropic material behavior is assumed for the FE modelling of the friction material (Figure 4.4.b). The independent elastic constants are Young's modulus and Poisson's ratio in the x-y plane E_p , ν_p ; shear modulus and Poisson's ratio in z-direction G_{pz} , ν_{pz} as well as the Young's modulus in z-direction E_z .

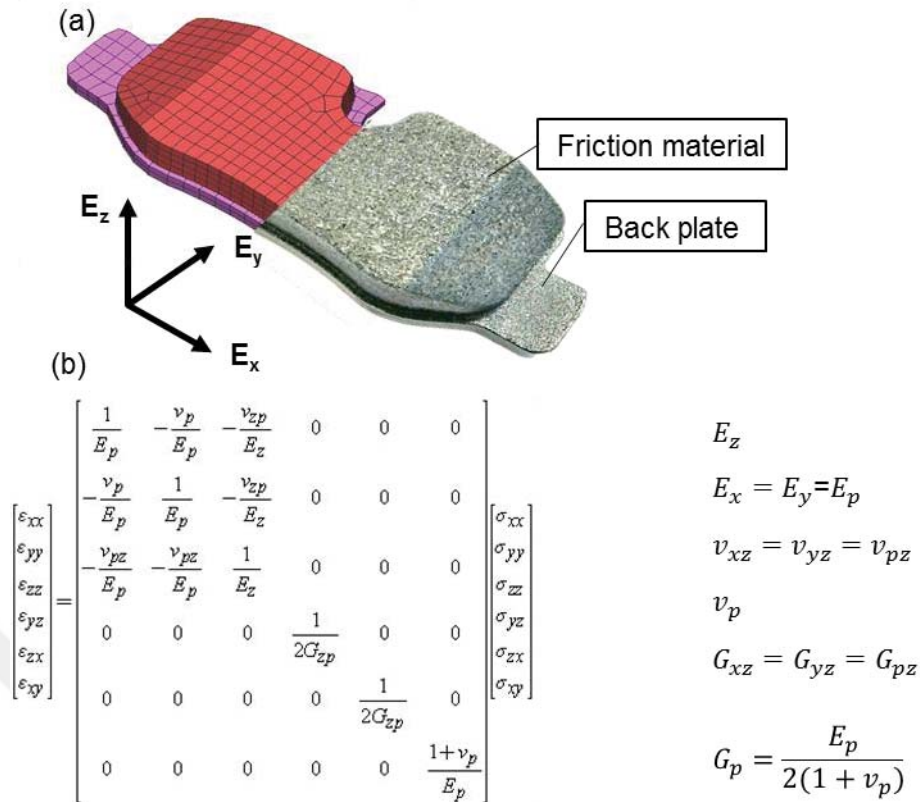


Figure 4.4: a) The brake pad b) The parameters of a transversely isotropic material

The model for the friction material of one brake pad consists of 1,344 hexa elements. The back plate is modelled with 698 hexa elements. In both cases, elements are of type C3D8I. The elastic material properties of steel are used to validate the back plate in FE model. Carvajal [Car16] presented a database with different friction material parameter sets which were obtained experimentally for ten different samples. Based on this database, an optimization of the friction material parameters is executed by applying a design of experiment (DoE). In the DoE, the upper and lower boundary conditions for the elastic constants are defined and 125 variants are run. For each variant, the difference in natural frequencies between numerical and experimental results is analyzed. The variants which provide an error of max. 2 % for three modes of the brake pad are considered for further evaluation. Further iterations for the optimization are conducted and four parameter sets are obtained (Table 4.1). The elastic constants in parameter sets are normalized based on the elastic constants of the material parameter set A. And the parameter set A is selected as a default. Normalization is done, because the material parameters derived by this procedure are regarded as confidential. Three modes are validated with max 1 % error in terms of mode shapes and natural frequencies (Figure 4.5). It is important to mention that there is no single set of elastic constant identified in the DoE which provides a best match and there might be other parameter sets which can be used for validation.

Table 4.1: The material parameter sets are obtained by DoE

Parameter set	$E_x=E_y$	E_z	ν_{xy}	$\nu_{xz}=\nu_{yz}$	$G_{xz}=G_{yz}$	G_{xy}
A (Default)	1	1	1	1	1	1
B	1	1.66	1	1	0.91	1
C	1.08	0.55	1	1	1	1.08
D	1	1.11	1	1	1	1

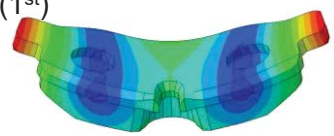
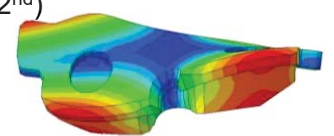



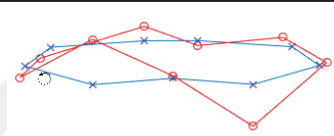
FEM	(1 st)  3,723 Hz	(2 nd)  5,558 Hz	(3 rd)  7,837 Hz
EMA	 3,720 Hz	 5,590 Hz	 7,780 Hz
Error	0.09%	-0.56%	0.73%
	Bending	Torsion	Bending

Figure 4.5: The natural frequencies and corresponding mode shapes of the brake pad

4.2.3 Carrier

The FE model of the carrier consists of 12,300 solid elements which are tetra elements (type C3D10). The material of the carrier is cast gray iron (GGG50) and its material elastic constants are tuned for the correlation between simulation and experiment results. Figure 4.6 illustrates the predicted mode shapes of the carrier in terms of mode shape and natural frequency. All natural frequencies and corresponding mode shapes of the carrier are well validated, except the natural frequency of the third mode shape. However, the mode shape itself is well predicted.

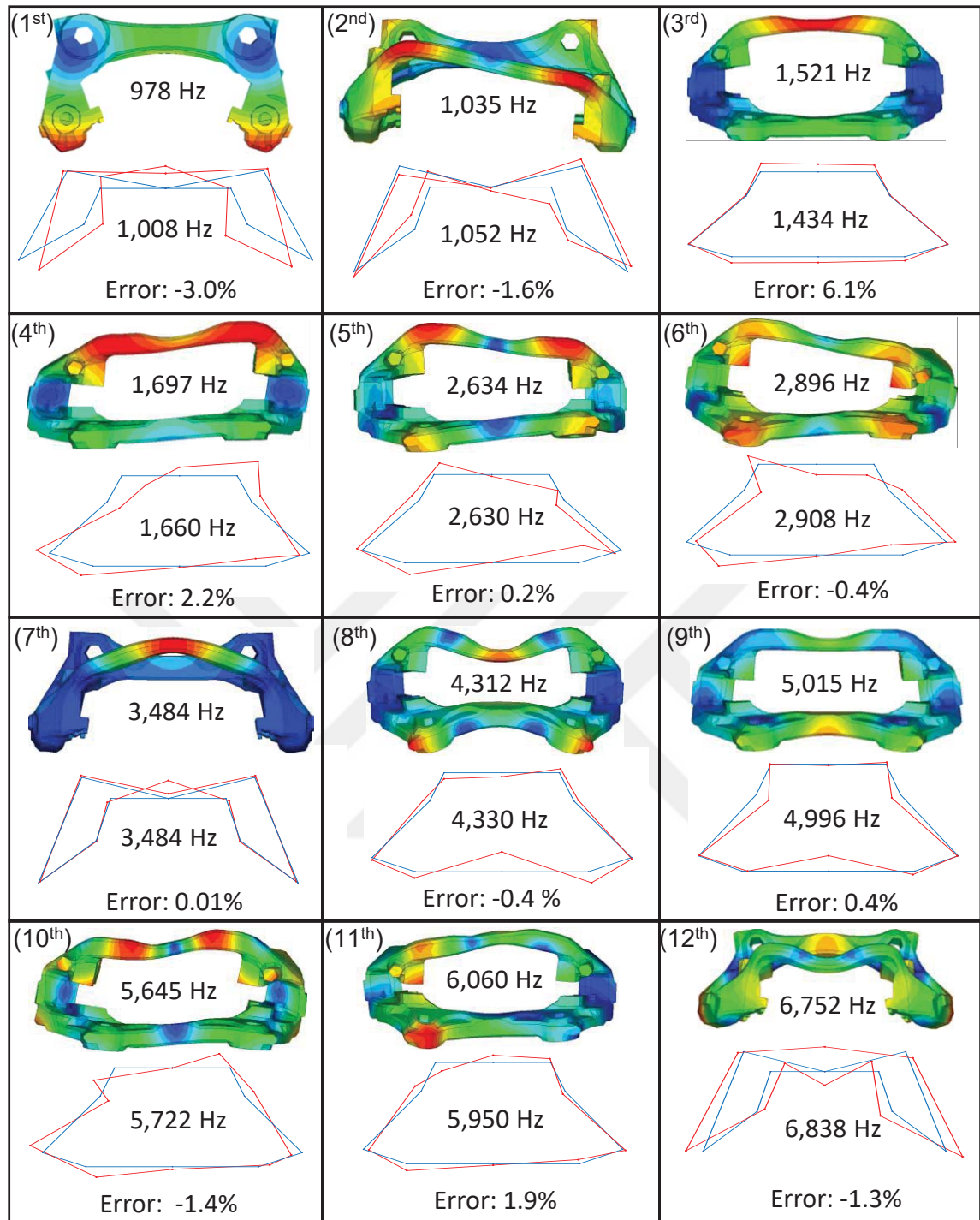


Figure 4.6: The natural frequencies and corresponding mode shapes of the carrier

4.2.4 Caliper

The FE model of the caliper consists of 21,768 tetra elements (type C3D10). The material of the caliper is GGG50 as for carrier. The geometry of the caliper is quite complex which causes the representation of its mode shapes to be challenging in two-dimensional space. In Figure 4.7, the parts of the caliper are named and numbered to conveniently explain the correlation

between the FE analysis and modal testing. The fingers of the caliper are critical parts in the context of the simulation due to their interactions with the outer brake pad. When braking occurs, these fingers apply forces on the brake pad and have a strong influence on the contact behavior between the brake pad and brake disc. Although the ears of the caliper do not have a direct effect on the contact between the brake pad and the disc, their dynamic behaviors are an indicator for matching mode shapes.

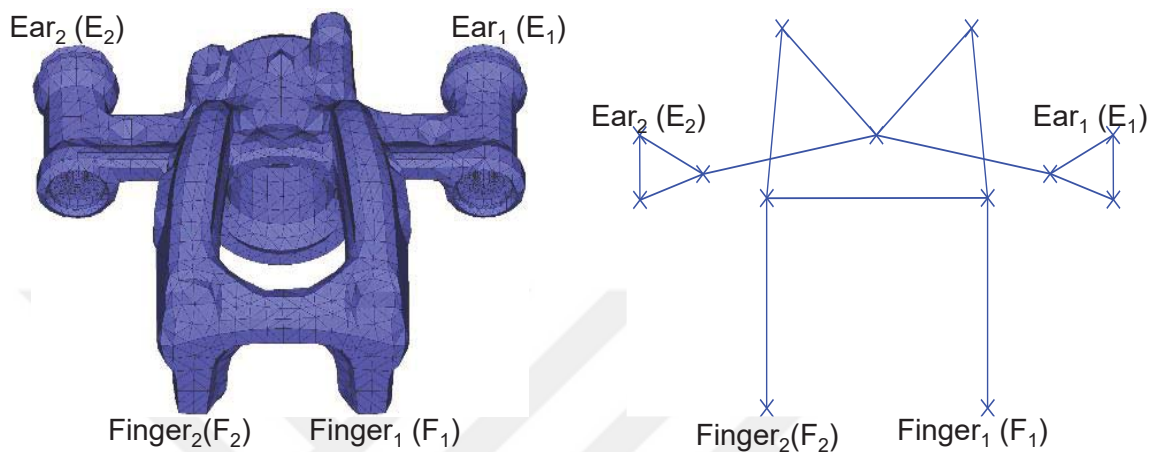


Figure 4.7: The ears and fingers of the caliper are on FE model and wire frame model

The validated mode shapes of the caliper are shown in Figure 4.8. In phase and out of phase behaviors of the ears are depicted by utilizing e_1 and e_2 which are perpendicular oriented to the image plane considering the mode shapes in FE model. If the ears move in phase, both e_1 and e_2 are illustrated in the same direction (Figure 4.8.b). If the ears move out of phase, their motion is illustrated as in Figure 4.8.a and Figure 4.8.c. The mode shapes obtained experimentally are depicted with the aid of a wire frame model, whereas the blue frame represents the undeformed state and the red frame the deformed state. Within the wire frame model, shifts in the location of the points (F_1, F_2, E_1, E_2) (reference state) are illustrated with the notations (f_1, f_2, e_1, e_2) (deformed state).

As depicted in Figure 4.8 the natural frequencies and mode shapes are well validated for all modes by the FE simulation. Except the first mode, the magnitude of error is less than 2%. In case of the first mode, a change of position of the first finger (Finger₁) cannot be confirmed in modal testing. A possible explanation may be, that the measuring point is located at an antinode or the finger₂ moves relatively less than the other one and therefore its movements cannot be measured accurately in modal testing. In addition, the finger₁ is indicated to move more than finger₂ in the FE simulation, which strengthens the possibility of an inaccurate measurement for finger₁ in the experimental modal testing. For all other mode shapes, the FE analysis and results of the modal testing show good correlations regarding the phase behavior

of the ears and fingers. Even the torsional motion of the ears is reproducible not only from the modal testing data but also in the FE model (Figure 4.8.d).

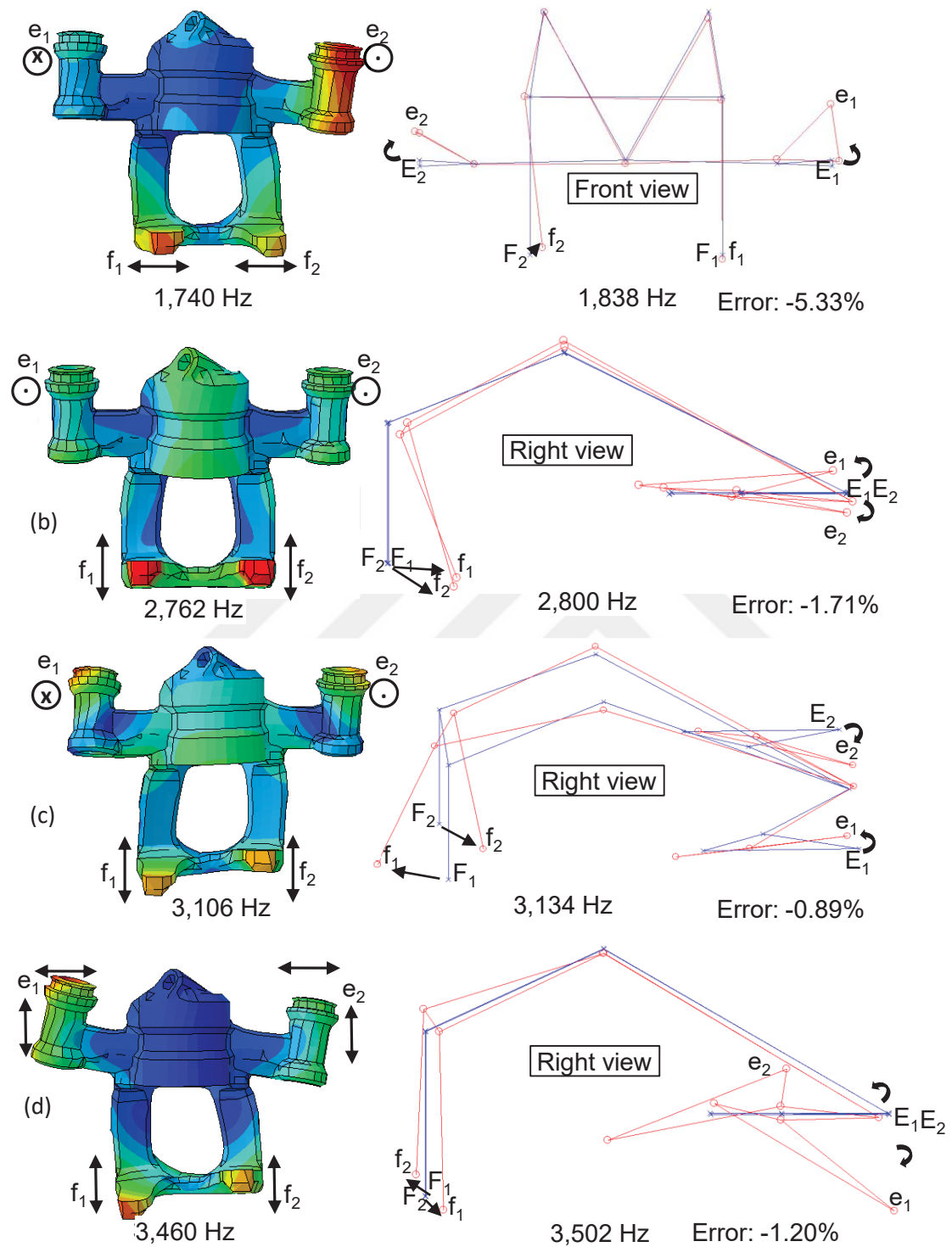


Figure 4.8: The natural frequencies and corresponding mode shapes of the caliper

4.3 Validation of Brake Assembly

In this subchapter, the validated brake components are incorporated in a virtual model of the brake assembly and their contact interactions are defined within the framework of Abaqus. The contact formulations of interacting surfaces are parametrized concerning the role of the surfaces (master or slave), contact discretization and tracking approach.

In this study, surface-to-surface contact discretization is utilized to model the interactions of the brake pad and the brake disc as well as of the caliper and the piston since the computation of an accurate stress distribution in these contacts is significant in CEA. In case of the pad/disc contact pair, the surface of the pad is selected as the slave surface and is meshed finer than the rotors surface. Coulomb friction model is defined for the contact pairs. Further information related to contact definitions is given in the Abaqus Manual [Aba14].

The modal analysis of the assembly is conducted by application of a force which equals a brake line pressure of 2 bar. The obtained natural frequencies and associated mode shapes of the assembly are compared with the ones attained in the experimental modal tests (Figure 4.9). Except the second mode of the assembly, the relative error in frequencies below 5%. In this study, to extract the mode shapes was challenging due to not only boundary conditions but also inadequate measurement points on the brake disc. The region where carrier, pad and caliper are coupled was restriction to perform modal testing on the disc. Hence, the possible peaks and valleys in this region could not be estimated. Nevertheless, the modal testing on the rest of the disc provides useful information to compare the mode shapes between experiment and FE results. Especially, the mode shapes of the first mode and the fourth mode in EMA are highly similar the ones in FE model.

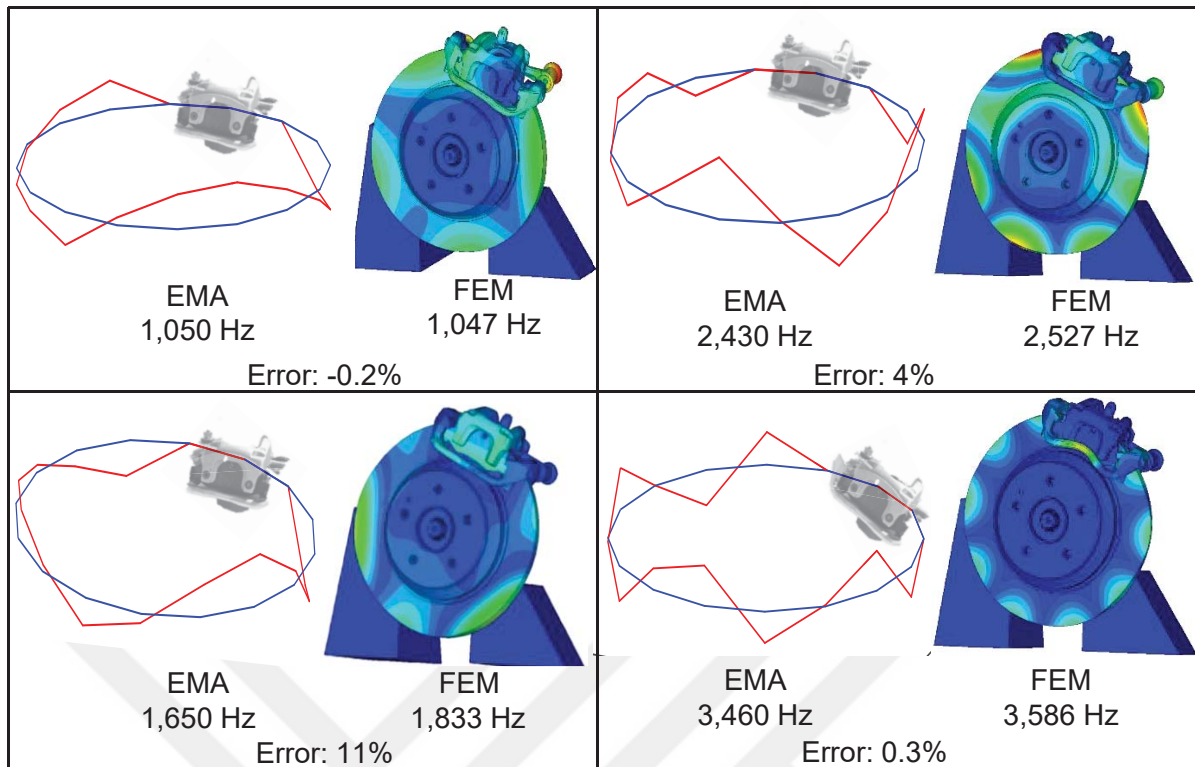


Figure 4.9: The natural frequencies and corresponding mode shapes of the assembly

5 Investigation of Disc Brake Squeal

5.1 Introduction

In this chapter, results of the experimentally and computationally investigation of the disc brake squeal phenomena are presented. Firstly, squeal propensity of a single brake assembly is studied on a test rig in a semi anechoic room. The brake pressure and rotational speed levels which cause a brake squeal are obtained. Secondly, a simulation method is built based on nonlinear static analysis followed by complex eigenvalues extraction [Kun03]. The unstable modes of the brake assembly which are associated with brake squeal are predicted by CEA.

5.2 Experimental Studies of Disc Brake Squeal

In this chapter, the experimental studies for the investigation of the brake squeal phenomena are explained. The section is divided into two parts: Methodology and Experimental Setup, Results.

5.2.1 Methodology and Experimental Setup

The methodology for the investigation of squeal is illustrated with the flowchart in Figure 5.1. The test starts with setting the rotational velocity at desired level. Then brake pressure is applied and kept constant at chosen level. If squeal is detected, the test is measured. Whether

squeal is observed or not, after each test the temperature on the friction disc is measured. If the measured temperature is higher than the desired value, the test system is left to cool down. When the temperature on the friction disc is below the chosen level, the investigation of squeal is continued. The succeeding tests can be performed with different velocity and pressure levels. In this study, the investigation of squeal test was started with maximum capacity of rotational speed. Then, the rotational velocity was decreased step by step, which was performed for different pressure levels.

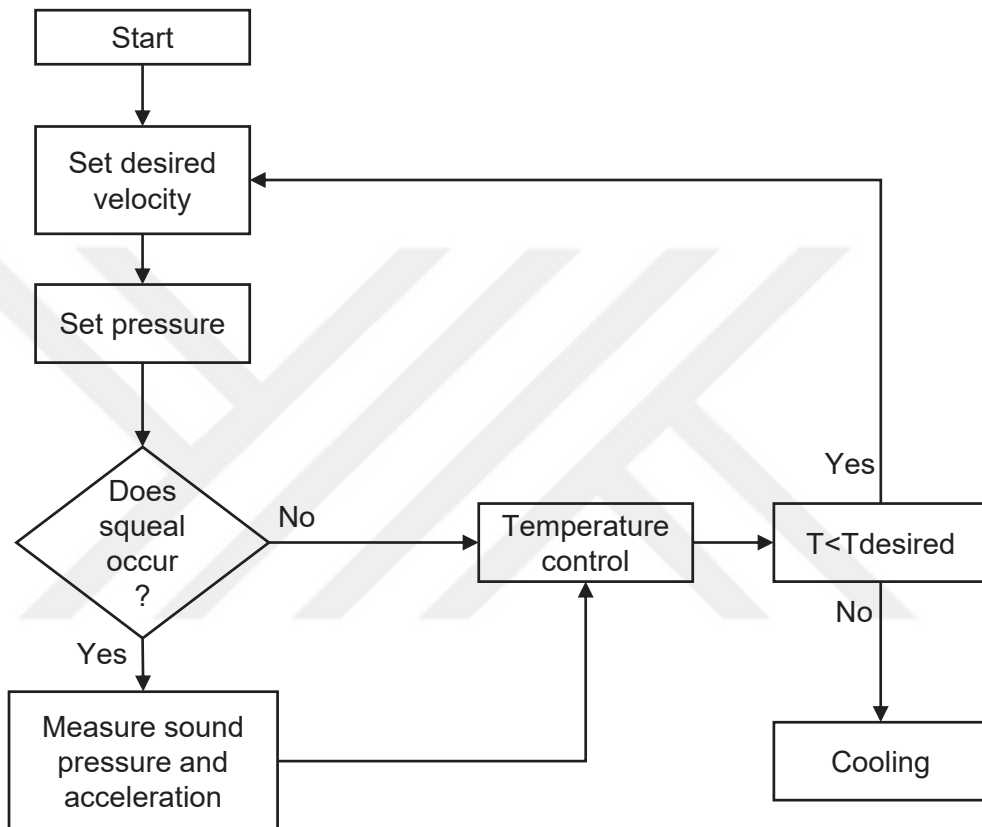


Figure 5.1: The flowchart for the description of the squeal investigation

The experimental set up is illustrated schematically in Figure 5.2. The brake pressure is applied to the brake assembly by means of a hydraulic master cylinder (2) which is actuated by a pneumatic cylinder (1). The rotation of the brake disc is generated by an AC motor (5) over a prop shaft (6). The AC motor is controlled by using an inverter (4) which enables to change a direct current to an alternating current. Hence, the rotational speed of the brake disc can be set for desired values.

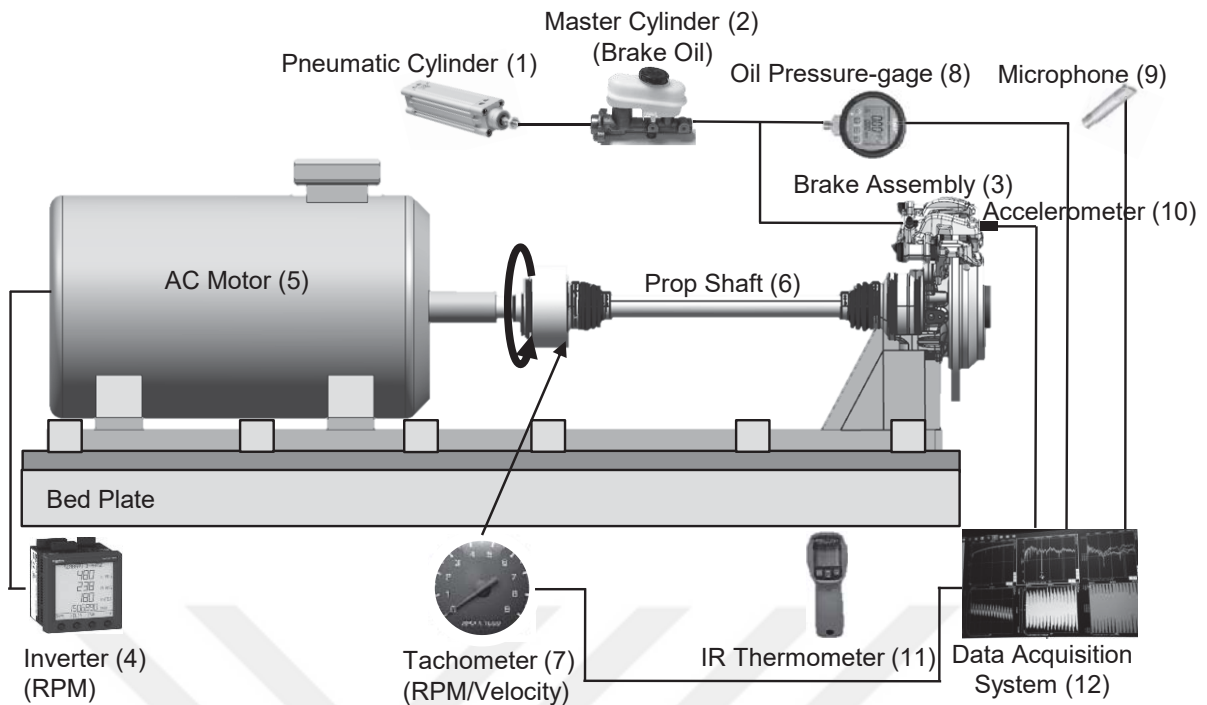


Figure 5.2: Schematic presentation of the test bench

During the experiments, the required output parameters are measured and collected into a data acquisition system (DAQ). The brake line pressure is measured through an oil pressure gauge type Keller with 16 bar range. A digital optical tachometer Monarch PLT200 is used to measure the rotational speed of the brake disc. The temperature of the brake disc is measured by using infrared thermometer with a sensitivity of ± 1.5 °C. The free-field $\frac{1}{2}$ " microphone type B&K 4189, which has a sensitivity 50 mV/Pa and frequency range 6.3-20,000 Hz, is placed 10 cm away from the disc and 50 cm high from the rotational axis of the disc according to SAE technical report [SAE J2521]. By using the microphone, sound pressure is measured. In addition, a uniaxial piezo-electric accelerometer type B&K 4506 which has a sensitivity 100mV/g is placed on the back plate in order to acquire the vibration signal at squeal events. The analogue signals provided by the listed sensors are digitized through a data acquisition system (DAQ) type Dewe-43. The sampling frequency is set at 20,000 Hz. To eliminate erroneous results caused by frequencies which are higher than the Nyquist frequency, an anti-aliasing filter (low pass filter) is employed.

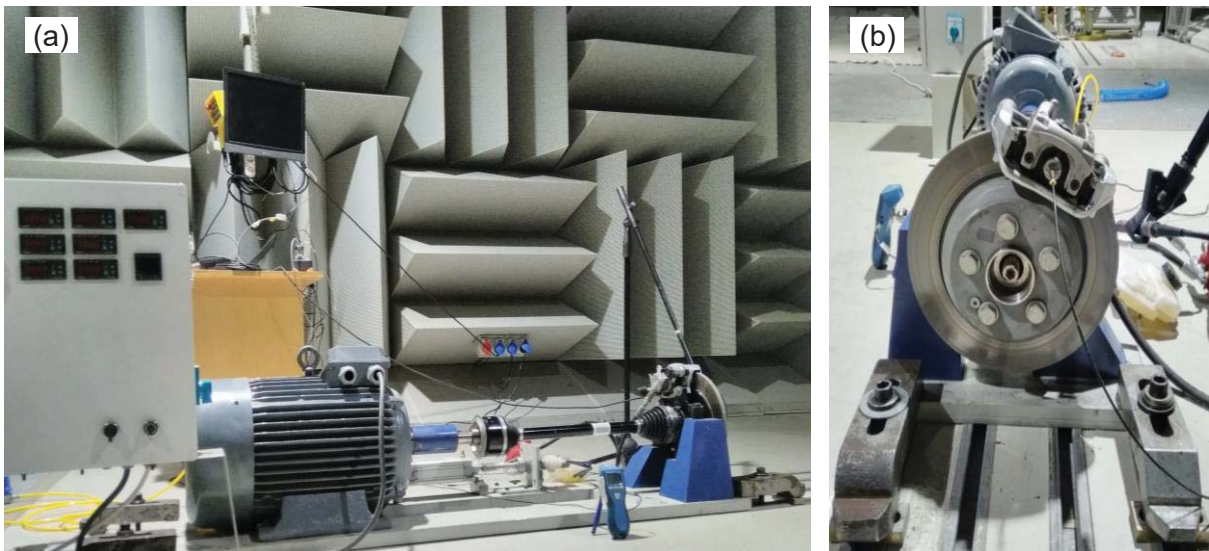


Figure 5.3: a) The test bench in the semi-anechoic room b) The front view of the test bench

The squeal experiments were conducted in a semi anechoic room located in the Automotive Technologies Research Center (OTAM) at Istanbul Technical University. The specially designed walls of the anechoic room absorb the sound waves emitted from the source and prevent the permeation of sound waves which originate from outside of the room. . A semi anechoic room is described as an anechoic room which has solid floor instead of isolated material. Performing a squeal test in semi anechoic room is aimed to execute acoustic measurements without noise (Figure 5.3.a). The test bench is fixed to the ground with clamping units as shown in Figure 5.3.b.

5.2.2 Results

Figure 5.4a shows an example for a constant speed braking at an initial rotating speed of 338 rpm and a brake line pressure between 0-5 bar. The acceleration data was collected at the outer back plate of the brake pad. The brake line pressure is plotted in the same figure to show how a change in brake line pressure effects the stability of the system considering the magnitude of the acceleration signal. The fluctuations in the pressure signals occur since vibrations of the caliper transfer into the brake fluid, which affects the brake line pressure. A Savitzky-Golay filter is employed for the smoothing of the pressure signal.

A spectrogram of the acceleration signal derived from an FFT is given in Figure 5.4.b. Hamming window with 70 % overlapping is applied to avoid leakage. The color bar represents the magnitude of the acceleration in logarithmic scale.

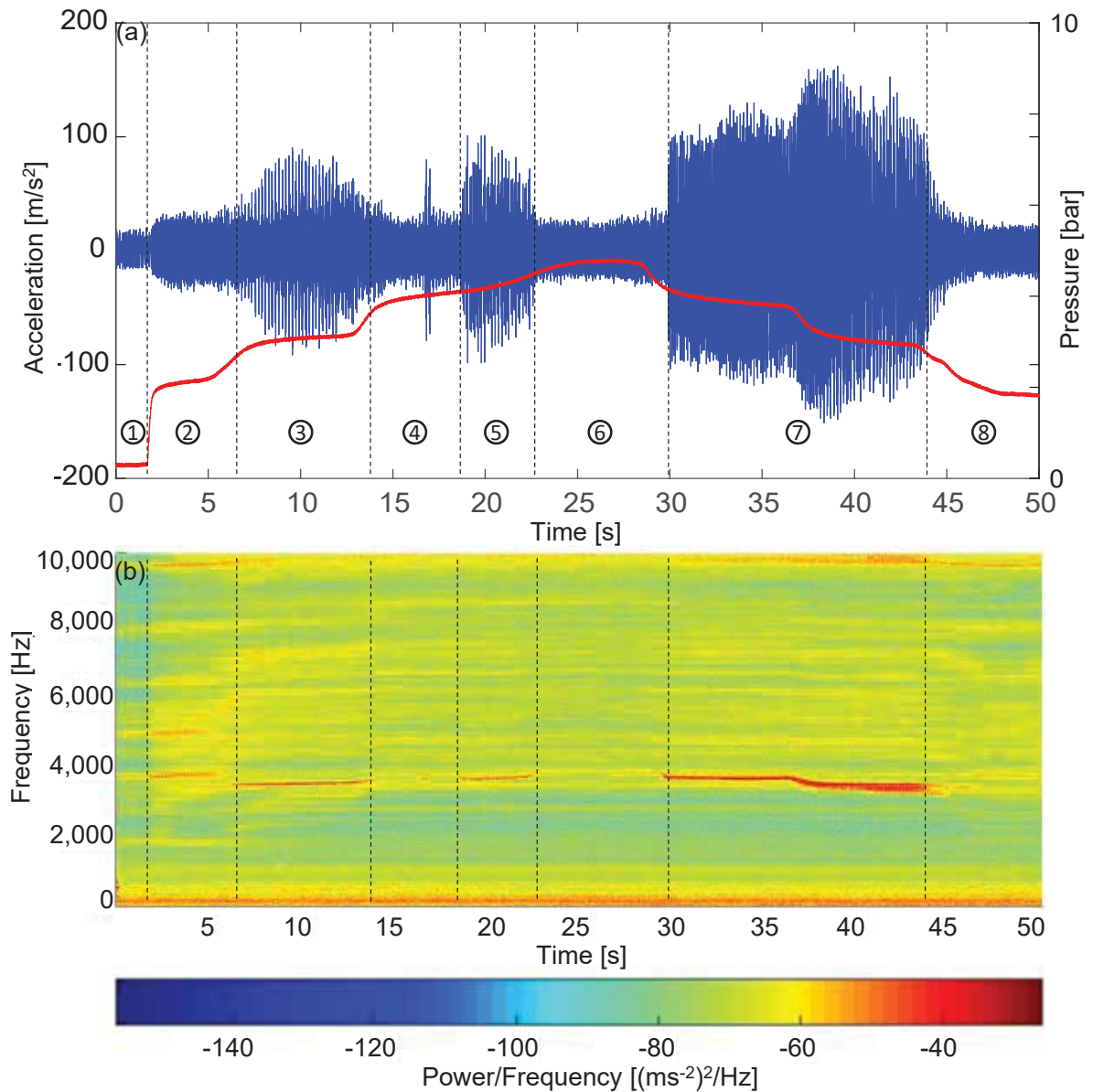


Figure 5.4: (a) The acceleration signal and brake line pressure in time domain (b) Short time Fourier transform of the acceleration signal

The signal is divided into eight sections to interpret the evaluation of the squeal event.

Section 1. From 0.0 s to 1.7 s: The brake line pressure is kept constant at 0.3 bar. The disc is able to rotate.

Section 2. From 1.7 to 6.3 s: The brake line pressure is gradually increased from 2.0 to 3.0 bar. All the frequencies up to 10,000 Hz are excited and a small squeal component is visible around 3,400 Hz. The squeal components in all sections, which can be detected by considering the lines showing high color density in spectrogram of acceleration data, are also confirmed by the spectrogram of sound data.

Section 3. From 6.3 to 14.1 s: A strong squeal component around 3,400 Hz can be seen clearly in this section when the pressure is increased from 3.0 to 4.0 bar.

Section 4. From 14.1 to 18.6 s: The squeal frequency of roughly 3,400 Hz disappears as the brake line pressure increases from 4.0 to 4.3 bar. However, a small squeal component is observed for a short time around 17.0 s.

Section 5. From 18.6 to 23.2 s: The squeal frequency shows up again as pressure increases from 4.3 to 4.7 bar. However, the magnitude of the frequency is not as high as in section 3 and fades before the pressure reaches 4.7 bar.

Section 6. From 23.2 to 30.0 s: In this section, the pressure is increased up to 5.0 bar and subsequently decreased to 4.3 bar. Although the pressure is increased, a squeal frequency is not monitored.

Section 7. From 30 to 44.1s: In this section, the pressure decreases from 4.3 to 3.0 bar. The squeal frequency appears again and shifts roughly from 3,600 Hz to 3,400 Hz when the pressure level is around 4.0 bar.

Section 8. From 44.1 to 50.0 s: The pressure is drained after 44.1 s. A squeal frequency is not detected and the data acquisition is stopped.

One possible explanation for the frequency shift in section 7 is that the applied pressure effects the stiffness of the contacts such as piston/back plate, friction material/disc and caliper/back plate. Hence, the squeal frequency might drop to about 3,400 Hz.

After the successful squeal tests, the pressure range which is prone to trigger squeal is determined. In this range, further experimental squeal investigations are conducted regarding different disc rotational speeds and brake line pressures. The obtained squeal events are depicted in terms of sound pressure level (SPL) in Figure 5.5. The squeal frequencies are detected as coarsely 2,400 Hz, 3,400 Hz, 6,800 Hz and 9,800 Hz. The dominant squeal frequency of 3,400 Hz is mostly observed at pressure levels between 3.3 and 4.3 bar while the rotating speed is between 40 and 60 rpm. The measured temperature of the brake disc was between 30 and 40 °C when the room temperature was between 20 and 25 °C.

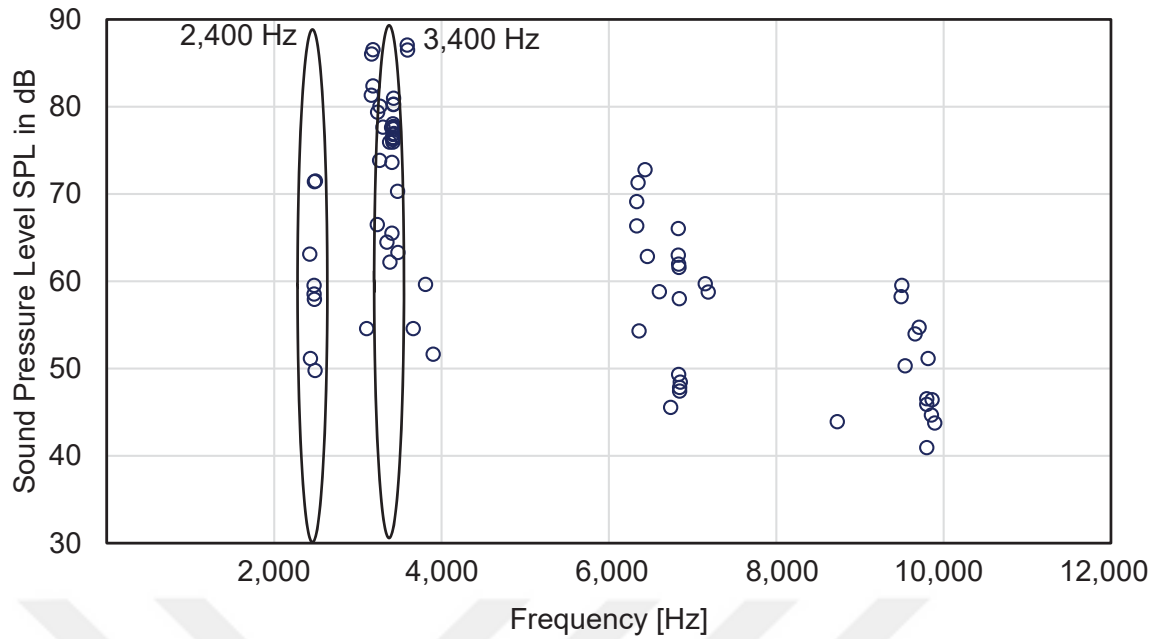


Figure 5.5: The measured squeals frequencies from the test bench

Figure 5.6 represents the effect of the brake line pressure on the squeal frequencies. As mentioned before, the brake system is prone to squeal between 3.3 and 4.3 bar. 23 out of 30 squeal events are observed between 3.8 bar and 4.3 bar. Two squeal events appear at 2,500 Hz in case of the pressure level is adjusted to 3.8 or 4.0 bar. Most squeal events are detected between roughly 3,100 Hz and 3,500 Hz.

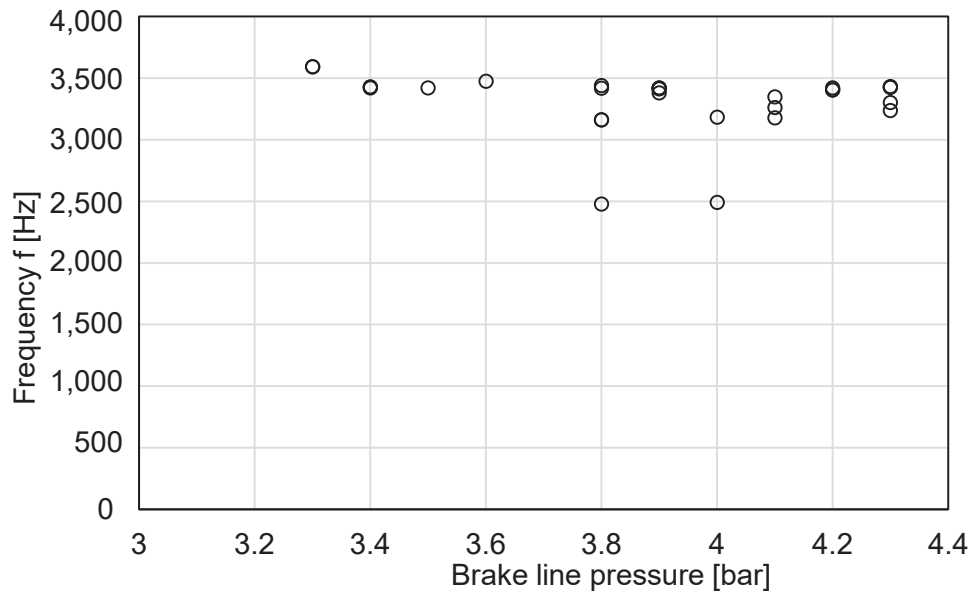


Figure 5.6: The Squeal frequencies versus different brake line pressure levels

The effect of the rotational speed on the squeal events is depicted in Figure 5.7. The squeal events are observed between 40 and 90 rpm. More than half of the squeal events are detected

between 40 and 50 rpm. Few squeal events are observed between 60 and 85 rpm. Except the events at 70 rpm, the squeal frequencies spread between roughly 3,100 Hz and 3,500 Hz.

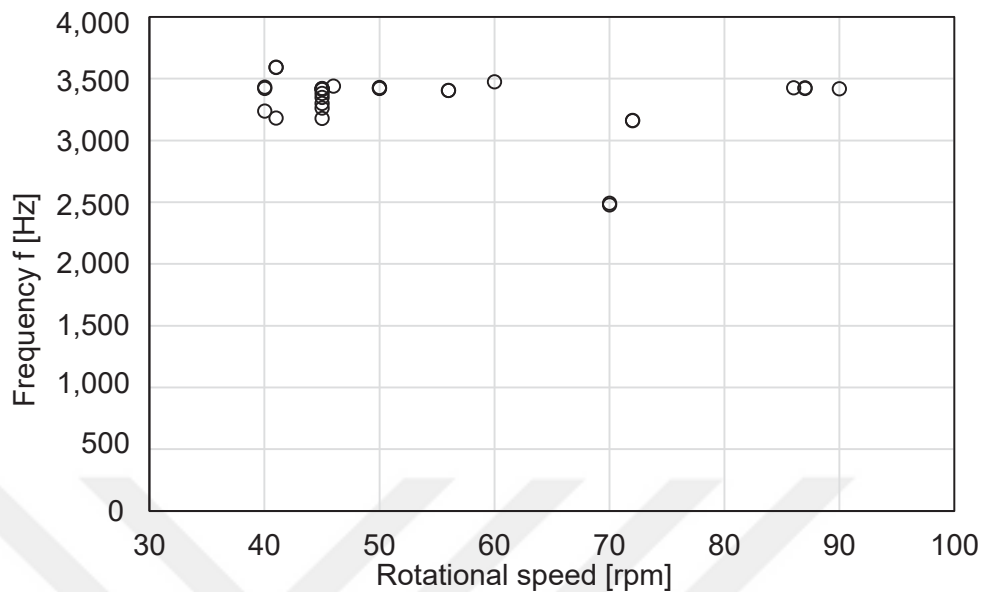


Figure 5.7: Squeal frequencies over rotational speed levels

5.3 Complex Eigenvalue Analysis

5.3.1 Brake Squeal Analysis Using FEM

To conduct an eigenvalue analysis of the disc brake assembly, the software suite Abaqus 6.13 is employed in consideration of the following simulation steps which are purposed by Kung et al [Kun03],

- Nonlinear static analysis for determination of the brake-line pressure
- Nonlinear static analysis to impose the rotational speed on the disc
- Normal mode analysis to extract the natural frequency of the undamped system
- Complex eigenvalue analysis that incorporate the effect of friction contact

For the prediction of brake squeal phenomena, the CEA is employed for a frequency range up to 10,000 Hz for a rotational speed of 45 rpm, a brake-line pressure of 4 bar and a constant friction coefficient of 0.4 in the contact zone of the brake pad and the brake disc. The material damping effects are neglected due to the lack of knowledge of their physical values.

5.3.2 Results

The CEA results are plotted in complex plane in Figure 5.8. As discussed in the chapter of state of the art the positive real part presents the unstable mode at associated frequency. The

predicted unstable modes, which are marked as red dots at 881 Hz, 3,514 Hz, 3,786 Hz, 4,325 Hz, 4,358 Hz, 4,363 Hz and 4,639 Hz, are prone to be brake squeal.

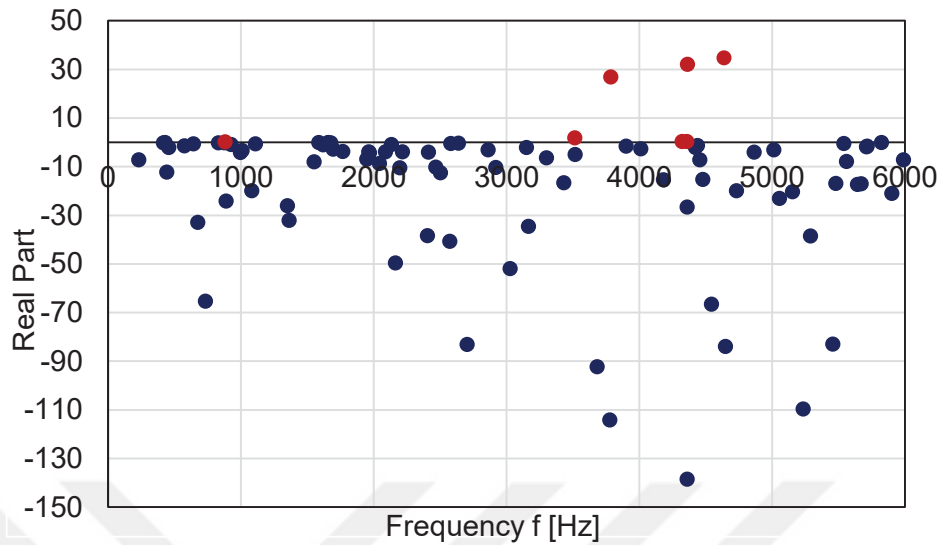


Figure 5.8: The extracted CEA values plotted in complex plane

Brake squeal is a phenomenon of dynamic instability which is caused mainly by the effect of friction between the brake pad and the brake disc. Therefore, the coefficient of friction is varied to study how the friction between the brake pad and the disc influences the stability of the system. The coefficient of friction is generally employed as 0.4. However, it can increase or decrease due to changing environmental conditions such as temperature, humidity, foreign particles in pad/disc contact area etc. Therefore, the coefficient of friction is altered in a range between 0.2 and 0.6 and the unstable modes are determined. These modes in relation to the coefficient of friction are plotted in Figure 5.9. It can be clearly seen that the number of the unstable modes increases as the friction coefficient increases. A possible explanation is that a higher friction coefficient results in higher frictional forces between pad and disc and the brake system becomes instable.

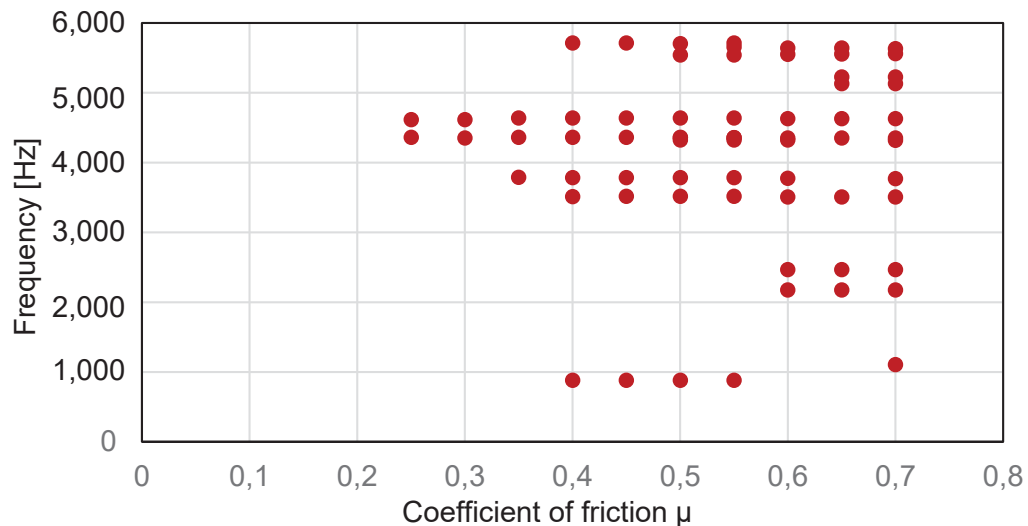


Figure 5.9: The effect of friction coefficient on stability of the brake system

The coefficient of friction 0.4 is critical for this FE model, in which the number of unstable modes increases up to seven. Besides the frequency of an unstable mode, the mode shape at the corresponding frequency must be taken into consideration to match the results of the CEA with the experimentally obtained squeal frequencies. The brake disc behaves like a “speaker” and emits the sound waves from its surface. Therefore, in the brake development field, engineers pay attention to the unstable modes which belong to the brake disc. Figure 5.10 illustrates two unstable modes of the evaluated brake system. For a better representation of the unstable mode in Figure 5.10.a, the caliper, the brake pad, the brake disc are hidden. This mode is related to the clip which is assigned to incorporate the brake pad and the carrier. In addition, the unstable modes at 3,786 Hz, 4,325 Hz, 4,358 Hz, 4,363 Hz and 4,639 Hz are also related to the clips. In this study, the unstable mode of the assembly in Figure 5.10.b, which is mainly dominated by the out of plane mode of the disc, is taken into consideration for the prediction of the squeal frequency at 3,400 Hz in experiments. This unstable mode consists of the 5-ND (nodal diameter) out of plane mode of the brake disc and the out of phase mode at ears and fingers of the caliper cf. chapter 4.2.4.

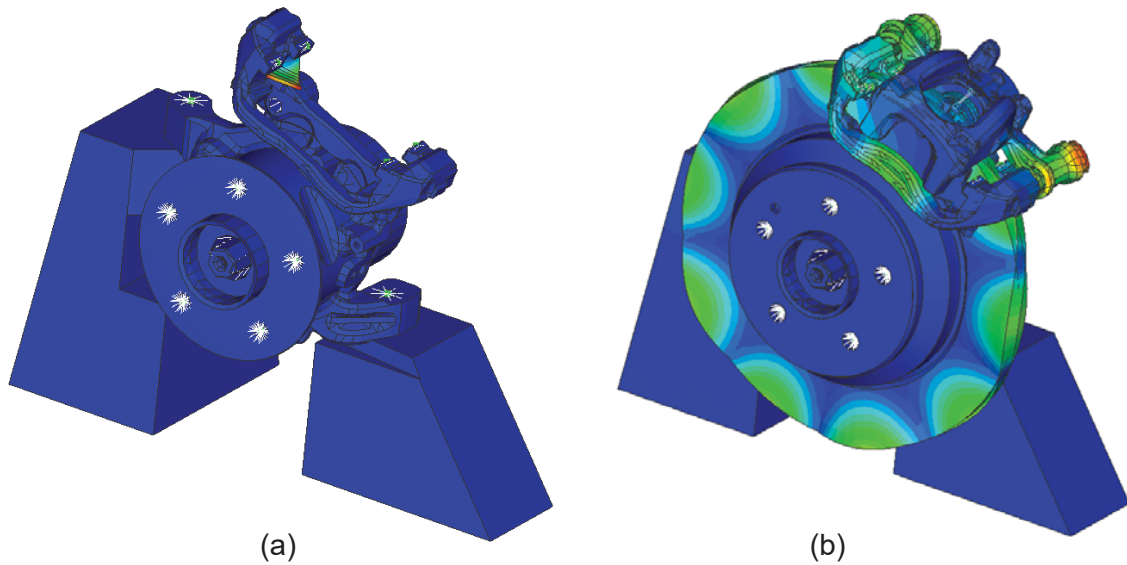


Figure 5.10: The unstable of the brake disc assembly a) at 881 Hz b) 3,514 Hz

6 Design Modifications and Sensitivity Analysis

6.1 Effect of Brake Pressure

The influence of brake pressure on the stability of the brake assembly was studied by utilization of CEA. The sensitivity analysis was performed for the brake pressure levels between 2-6 bar whilst other parameters were kept constant. The rotational speed was set 45 rpm and the coefficient of friction was kept at 0.4. The calculated frequencies of the unstable modes were plotted versus corresponding pressure level (Figure 6.1). It must be remembered that squeal is highly predicted by the unstable mode of the disc. Therefore, the instability of the brake system which is dominated by the unstable mode of the disc is focused in this study. The selected unstable mode, which is correlated with dominant squeal frequency in chapter 6.2.3, are depicted by using different marker on the graph. It is important to mention that the dominant squeal frequency, which is round 3,400 Hz in experimental tests, was also monitored in this range. The correlation between in CEA and experiment results well obtained. In Figure 6.1, it can be clearly seen that the selected unstable mode is detected when the pressure level is set a range of 3 and 4 bar. This mode cannot be observed outside of this range. The natural frequency of the selected mode increases as the pressure increases. The calculated frequency of the selected unstable mode at 4 bar is 10 Hz higher than the one at 3 bar. It is important to mention that the dominant squeal frequency, which is round 3,400 Hz in experimental tests, was also monitored in this range. The correlation between in CEA and experiment results for the mentioned pressure range well obtained.

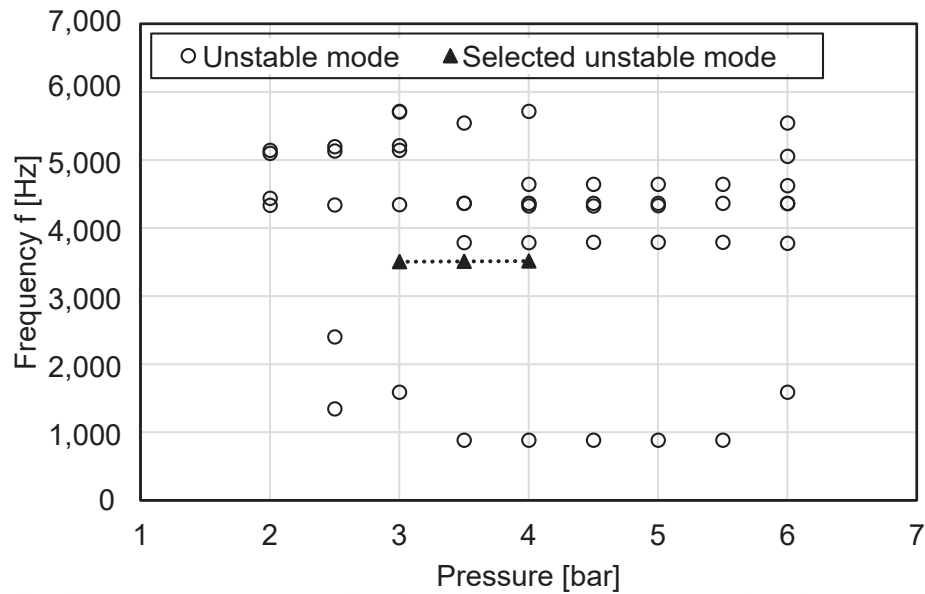


Figure 6.1: Effect of brake pressure on the stability of the brake system in CEA (The coefficient of friction is $\mu=0.4$ and rotational speed is 45 rpm)

6.2 Effect of Elastic Modulus of the Friction Material

At the validation stage of the brake pad in Chapter 4, different material parameter sets which provide minimum relative error in natural frequencies of the pad were obtained. The parameter set A has been employed in CEA so far, however the effect of the other parameter sets has not been considered yet. In this chapter, the influence of the other parameter sets on the stability of the brake system is discussed by performing CEA. Parameter sets B and C provide less number of predicted unstable modes than sets A and D. In addition, the instability at 3,514 Hz is suppressed by using the sets B and C. When the set A and Set D compared, the only difference in these sets is the value of the elastic constant in out of plane direction, which is the direction perpendicular to transversal plane. Roughly 10% increase in the elastic modulus increases the value of the real part drastically at 3,514 Hz. The stiffer elastic modulus in out of plane direction of the pad lead the system instability. As discussed before, the experimental test for the characterization of the friction material is critical for the validation of the simulation model.

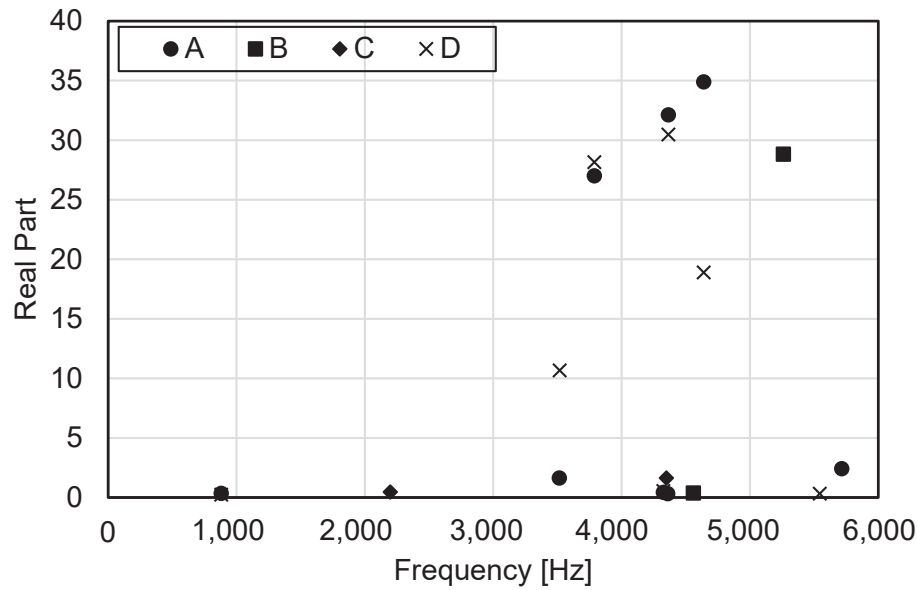


Figure 6.2: The influence of the different material parameter sets of the friction material on instability of the assembly in CEA

6.3 Geometry Modifications of the Brake Pad

In this study, the design modifications on brake pad were performed via cutting the slots on the friction material. The chief aim of these configurations is to change the coupling effect between the disc and the pads. In addition, the slots configurations are performed to change the frequency of the brake pad for its bending model [Gha11]. The applied slot configurations on the real pads and their FE model, which are center slot model (CS) and double slot model (DS), are illustrated in Figure 6.3. The efficiency of these configurations for the squeal treatment were compared with the results obtained with baseline model (B). The investigation was conducted in CEA by setting brake pressure 4 bar, rotational speed 80 rpm and coefficient of friction $\mu=0.6$. Afterwards, the slot configurations were investigated experimentally by conducting five squeal tests for each configuration. The squeal experiments were performed with the same operational conditions, which are brake line pressure round 4 bar and rotational speed round 80 rpm. Between the measurements in each case, the rotational velocity of the disc was changed up or down and set again at 80 rpm. Hence, the contact condition between pad and disc was changed between the measurements performed in each case and the repeatability of the squeal measurements with the same operational conditions were examined. The results of CEA and experiments are shown in Figure 6.4. According to the results in CEA, both configurations shows improvement to reduce the instability of the system considering the decrease in the value of real part. However, a significant change in natural frequencies cannot be seen when the slotted models are compared with the base line model. The evaluated natural frequency in baseline model is 3,514 Hz whilst the natural frequencies are 3,510 Hz in center slot and double slot models. In squeal tests, the comparison between the models are

interpreted in terms of a decrease in SPL. The average measured squeal frequencies are 3,472 Hz, 3448 Hz and 3,304 Hz for baseline, center slot and double slot models respectively. The 5 % decrease in the squeal frequency is remarkable between DS and B. The sound pressure level decreases in squeal events performed for the configured models as compared to the baseline model. The decrease in average SPL is round 10% for CS whilst it is round %15 for DS. It is apparent that the application of the slots on the friction material shows good results in CEA in terms of the reduction of the instability, which is in good agreement with the previous works done by Ghazaly [Gha11]. In addition, in this study, the parallel improvement is observed in the squeal tests with respect to the decrease in SPL. These findings are promising to work on the structural modifications of the pad in detail by considering the different dimensions and geometries.

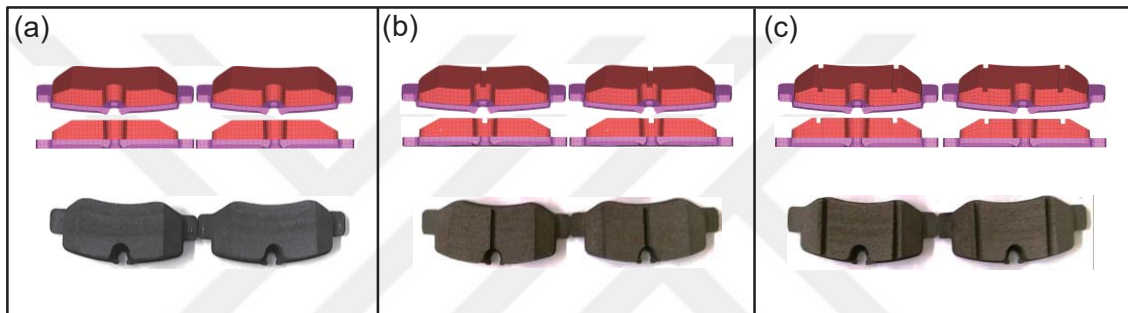


Figure 6.3: Geometry modifications on the brake pad a) Baseline b) Center slot c) Double slot (The width and the depth of the slots are 3mm)

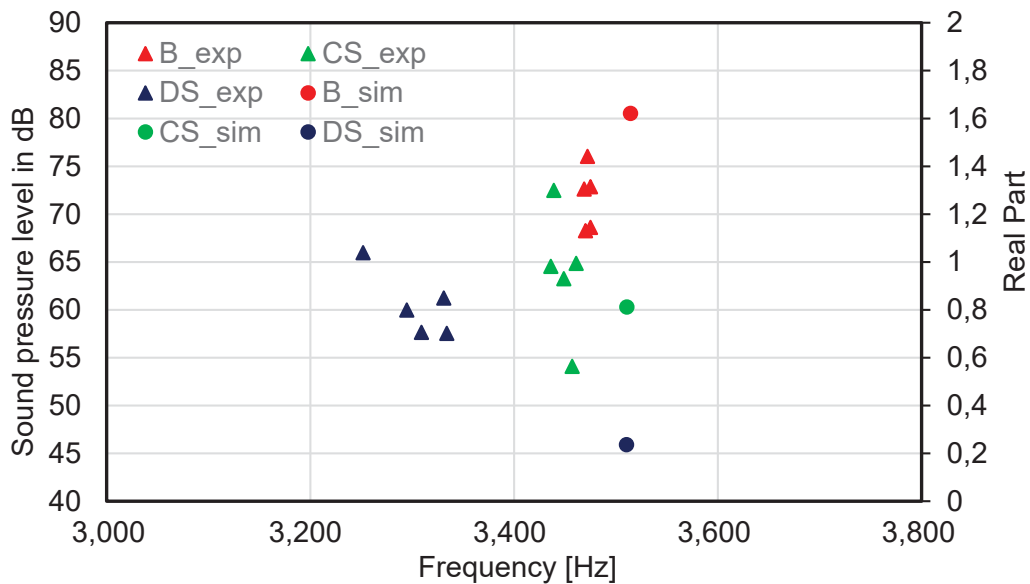


Figure 6.4: The influence of the geometry modifications on instability of the brake system

7 Conclusions

Within the scope of this thesis, a simulation methodology was developed for the investigation of brake squeal in the brake system of the lightweight commercial vehicle. The investigation was managed not only experimental studies but also FEM.

In chapter 1, a brief introduction of the brake systems was presented. The classifications of brake noises were explained and the importance of squeal in the view of automotive manufacturers was highlighted. After common approaches implemented to treat squeal were shortly discussed, the objectives of the thesis were expressed.

In chapter 2, the common squeal mechanisms in literature were described shortly. Afterwards, the approaches followed to investigate squeal were analyzed. Finally, the treatments have been performed by authors in brake industry were given.

In chapter 3, experimental modal analysis (EMA) was performed for the brake components (disc, brake pad, carrier and caliper) by utilization of the rowing hammer technique. Thus, the mode shapes and the corresponding natural frequencies were extracted. These results were the backbone of the thesis, because the results of the modal analysis were used for the validation of the FE model in succeeding chapter. In addition, EMA was performed for the brake assembly as well.

In chapter 4, normal modal analysis (NMA) was performed at component level. The FE models of the components were well correlated with the experiment results in terms of natural frequency and mode shape. At the assembly level, the mode shapes and the natural frequencies were also well predicted.

In chapter 5, squeal tests were conducted in semi-anechoic room. During the experiments, acceleration and sound pressure signals were collected to attain the dynamic and acoustic modes of the brake system. The operational conditions (brake line pressure and velocity) which lead to squeal were obtained. The obtained operational conditions and other working conditions (friction, contacts, connections among the components and etc.) were implemented into the simulation model. Complex Eigenvalue Analysis (CEA) were utilized to predict the instability of the brake model. The sensitivity analysis for the coefficient of friction was performed in CEA. An increase in the number of predicted unstable modes was observed as the coefficient of the friction increases. The simulation model was well validated according to the results of the squeal tests. The dominant squeal frequency monitored in tests was well predicted in CEA.

In chapter 6, the sensitivity analysis in CEA was performed for brake line pressure. It was observed that the predicted unstable mode at around 3,514 Hz which is associated with the dominant squeal frequency appears between 3 and 4 bars. This trend was also observed in

squeal tests. Secondly, the sensitivity analysis in CEA was conducted for the friction material by employing the different material parameter sets. It was observed that the parameter sets provide different dynamic characteristics for the system, although they provide close results for the modal validation of the friction material in chapter 4. The major finding was that 10% increase in elastic modulus of the friction material in out of plane direction increases the real part of the unstable mode at 3,514 Hz in CEA. Thirdly, a design suggestion for the reduction of squeal was given by proposing the slot configurations on the friction material. After promising results for the reduction of squeal were obtained in CEA, the prototype of the designs was attained. The squeal tests were performed with these designs. The improvements obtained in CEA were also detected in squeal tests.

Naturally, as it happens in each scientific study, this thesis brought new discussions for the further investigations. The conducted DoE for the validation of the friction material showed that there are several parameters sets which meet with the results of experimental modal analysis, although the difference in the elastic constants between these parameter sets is too much. Therefore, the characterization test for the friction material is suggested to obtain its material parameters. In CEA analysis, it was observed that there are a lot of predicted unstable modes which belong the clips connecting the brake pads to the carrier. In future works, the modelling of the clips and sensitivity analysis for their interactions with other components are suggested.

8 Bibliography

- [Aba14] ABAQUS Documentation, Dassault Systèmes, Providence, RI, USA 2014
- [Avi14] Avitabile, P.: Modal Space - Back to Basics: SEM Experimental Techniques, 2014
- [Baj04] Bajer, A.; Belsky, V.; Kung, S.: The Influence of Friction-Induced Damping and Nonlinear Effects on Brake Squeal Analysis. SAE Technical Paper, 2004
- [Bak05] Bakar A.: Modelling and Simulation of Disc Brake Contact Analysis and Squeal. PhD Thesis, University of Liverpool, 2005
- [Bas13] Bashery, N. M. G.: Study on automotive disc brake squeal using finite element analysis and design of experiments. Doctor of Philosophy, Anna University, 2013
- [Car16] Carvajal S.: Strategies in the simulation and optimization of brake comfort. PERMAS Users' Conference, 2016
- [Che09] Chen, F.: Automotive disk brake squeal: An overview. SAE Technical Paper, 2009
- [Cun02] Cunefare, K. A.; Graf A. J.: Experimental Active Control of Automotive Disc Brake Rotor Squeal Using Dither. Journal of Sound and Vibration 250, 4 (2002) 579-590
- [Day14] Day, A.: Braking of Road Vehicles. Elsevier, (2014) 343-384
- [Dai08] Dai Y.; Lim T.C.: Suppression of brake squeal noise applying finite element brake and pad model enhanced by spectral-based assurance criteria. Applied Acoustics, 69, 3 (2008) 196-214
- [Døs88] Døssing, Ole. Structural testing. Brüel & Kjær, 1988
- [Ewi00] Ewins, D. J.: Modal testing. Theory, practice, and application. Research Studies Press, 2000
- [Fie93] Fieldhouse, J. D.; Newcomb, P.: The Application of Holographic Interferometry to the Study of Disc Brake Noise. SAE Technical Paper, 1993

-
- [Fos61] Fosberry, R. A. C.; Holubecki Z.; Disc brake squeal: its mechanism and suppression. Motor Industry Research Association, 1961
- [Gha11] Ghazaly, N. M.: Study on Automotive Disc Brake Squeal Using Finite Element Analysis and Design of Experiments. Diss. PhD. Thesis, Department of Mechanical Engineering, Anna University, India, 2011
- [Hal16] Halderman, J. D.; Chase D. M.: Automotive brake systems. Prentice Hall, 2016
- [Har98] Harper, G. A.: Brakes and friction materials: the history and development of the technologies. Mechanical Engineering Publications Limited, 1998
- [Hof02] Hoffmann, F.; Fischer M.; Allgaier R.; Gaul, L.; A minimal model for studying properties of the mode-coupling type instability in friction induced oscillations. Mechanics Research Communications, 29, 4 (2002) 197-205
- [Ibr94] Ibrahim, R. A.: Friction-induced vibration, chatter, squeal, and chaos—part II: dynamics and modeling. Applied Mechanics Reviews, 47, 7 (1994) 227-253
- [Ish96] Ishihara, N.; Masaaki N.; Hidetoshi S.: Experimental Analysis of low-frequency brake squeal Noise. SAE Technical Paper, 1996
- [Jac03] Jacobsson, H.: Aspects of disc brake judder. Proceedings of the Institution of Mechanical Engineers, Part D: Journal of Automobile Engineering, 217, 6 (2003) 419-430
- [Jar63] Jarvis, R. P.; Mills B.; Vibrations induced by dry friction.” proceedings of the Institution of mechanical Engineers, 178, 1 (1963) 847-857
- [Jun08] Junior, M. T.; Gerges S., Jordan R.: Analysis of brake squeal noise using the finite element method: a parametric study. Applied Acoustics 69, 2 (2008) 147-162
- [Kin03] Kinkaid, N. M.; O. M. O'reilly; P. Papadopoulos. Automotive disc brake squeal. Journal of sound and vibration. 267, 1 (2003), 105-166
- [Kum04] Kumamoto, F.; Kawai K.; Baba H.: A study on relationship between pad restraint condition and brake squeal generation. SAE Technical Paper, 2004

-
- [Kun03] Kung, S.; Stelzer G.; Belsky G. Bajer A.: Brake squeal analysis incorporating contact conditions and other nonlinear effects. SAE Technical Paper, 2003
- [Lil89] Liles, G. D.: Analysis of disc brake squeal using finite element methods. SAE Technical Paper, 2003
- [Liu00] Liu, W.; Pfeifer J: Reducing high frequency disc brake squeal by pad shape optimization. SAE Technical Paper, 2000
- [Mas08] Massi, F., Giannini O.: slightEffect of damping on the propensity of squeal instability: An experimental investigation. The Journal of the Acoustical Society of America, 123, 4 (2008) 2017-2023
- [Mil38] Mills, H. R.: Brake squeak. Institution of Automobile Engineers, 1938
- [Nob15] Nobari, A.: Uncertainty Quantification of Brake Squeal Instability via Surrogate Modelling. Doctor in Philosophy, University of Liverpool, 2015
- [Nor72] North, M. R.: Disc brake squeal: a theoretical model. Hillington Press, 1972
- [Pap07] Papinniemi, A.: Vibro-acoustic Studies of Brake Squeal Noise. Doctor of Philosophy, The University of New South Wales, 2007
- [Pap02] Papinniemi, A., Lai J.; Zhao J., Loader L.: Brake squeal: a literature review. Applied acoustics, 63, 4 (2002) 391-400
- [Ree00] Reeves, M.; Taylor N.; Edwards C.; Williams D.; Buckberry C. H.; A study of brake disc modal behaviour during squeal generation using high-speed electronic speckle pattern interferometry and near-field sound pressure measurements." Proceedings of the Institution of Mechanical Engineers, Part D: Journal of Automobile Engineering, 214, 3 (2000) 285-296
- [Rhe89] Rhee, S. K.; Tsang, P. H. S.; Wang, Y. S.: Friction-induced noise and vibration of disc brakes. Wear 133, 1 (1989) 39-45
- [SAE J2521] SAE J2521 -Technical Report. SAE International, 2013
- [Spu61] Spurr, Robb T.; A theory of brake squeal. Proceedings of the Institution of Mechanical Engineers: Automobile Division, 15, 1 (1961) 33-52

9 List of Figures

Figure 1.1: Two main caliper design are shown schematically a) caliper b) sliding caliper. This figure is adapted from [Kin03].	8
Figure 1.2: The classification of brake noise [Dai08].	9
Figure 2.1: The flow diagram of signal processing for impact test [Avi14].	14
Figure 2.2: Output spectrum is obtained by linear multiplication of input spectrum and FRF. This figure is adapted from [Døs88].	15
Figure 2.3: FRFs of a cantilever beam obtained at different excitation and response points. This figure is adapted from [Avi14].	16
Figure 2.4: Definition of master and slave surfaces [Aba14].	17
Figure 2.5: Schematic of a spring-mass-damper system on a sliding surface [Kin03].	19
Figure 2.6: a) Spurr's test setup for sprag slip a) The simplified model of Spurr's test setup, adapted from [Kin03].	20
Figure 2.7: The model of Jarvis and Mils [Jar63].	21
Figure 2.8: System studied by Hoffmann et. al [Kin03].	21
Figure 2.9: According to the Hoffman's model, changes in (a) natural frequencies and (b) real parts, adapted from [Nob15].	22
Figure 3.1: The nodes and antinodes on two different mode shapes of the disc	26
Figure 3.2: a) The experimental setup for the disc b) The measurement points on the disc.	27
Figure 3.3: The results of two modal testing on the disc with a) FRFs b) Coherence functions	28
Figure 3.4: The experimental setup for the brake pad	29
Figure 3.5: a) The brake pad and b) The measurement points on the back plate	29
Figure 3.6: The results of two modal testing on the brake pad with a) FRFs b) coherence functions	30
Figure 3.7: The FRFs of eight brake pads.	31
Figure 3.8: a) The experimental setup for the carrier b) The measurement points on the carrier	31
Figure 3.9: The results of two modal testing on the carrier with a) FRFs b) Coherence functions	33

Figure 3.10: a) The experimental setup for the caliper b) The measurement points on the caliper	33
Figure 3.11: The results of two modal testing on the caliper with a) FRFs b) Coherence functions	34
Figure 3.12: The experimental setup for the brake assembly and the measurement points.	35
Figure 3.13: FRF of the brake assembly is plotted regarding the driving point 9 and 2 bar brake line pressure	36
Figure 4.1: The CAD model of the brake disc in this study	37
Figure 4.2: The validation steps of the brake components	38
Figure 4.3: The natural frequencies and corresponding mode shapes of the disc	39
Figure 4.4: a) The brake pad b) The parameters of a transversely isotropic material	40
Figure 4.5: The natural frequencies and corresponding mode shapes of the brake pad	41
Figure 4.6: The natural frequencies and corresponding mode shapes of the carrier	42
Figure 4.7: The ears and fingers of the caliper are on FE model and wire frame model	43
Figure 4.8: The natural frequencies and corresponding mode shapes of the caliper	44
Figure 4.9: The natural frequencies and corresponding mode shapes of the assembly	46
Figure 5.1: The flowchart for the description of the squeal investigation	47
Figure 5.2: Schematic presentation of the test bench	48
Figure 5.3: a) The test bench in the semi-anechoic room b) The front view of the test bench	49
Figure 5.5: The measured squeals frequencies from the test bench	52
Figure 5.6: The Squeal frequencies versus different brake line pressure levels	52
Figure 5.7: Squeal frequencies over rotational speed levels	53
Figure 5.8: The extracted CEA values plotted in complex plane	54
Figure 5.9: The effect of friction coefficient on stability of the brake system	55
Figure 5.10: The unstable of the brake disc assembly a) at 881 Hz b) 3514 Hz	56
Figure 6.1: Effect of brake pressure on the stability of the brake system in CEA (The coefficient of friction is $\mu=0.4$ and rotational speed is 45 rpm)	57
Figure 6.2: The influence of the different material parameter sets of the friction material on instability of the assembly in CEA	58

Figure 6.3: Geometry modifications on the brake pad a) Baseline b) Center slot c) Double slot
(The width and the depth of the slots are 3mm) 59

Figure 6.4: The influence of the geometry modifications on instability of the brake system.. 59

10 List of Tables

Tabel 3.1: The natural frequencies for the modes of the disc..... 28

Table 3.2: The natural frequencies for the modes of the carrier 32

Table 3.2: The natural frequencies for the modes of the caliper 34

Table 4.1: The material parameter sets are obtained by DoE 41



Declaration in Lieu of Oath

Tozkoparan, Ömer Anıl

181749

Last name, First name

Student ID:

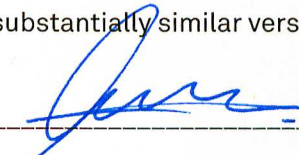
I hereby declare in lieu of oath that I have composed the enclosed bachelor's/master's* thesis entitled "Development of Acoustic Simulation Method for Brake Squeal based on Experiments in the Test Bench"

entirely on my own and without any inadmissible help from outside. I have not used any outside sources without declaration in the text. Any concepts or quotations applicable to these sources are clearly attributed to them.

This master's thesis has not been submitted in the same or substantially similar version, not even in part, to any other authority for grading.

Izmir, 01.06.2017

Place, date


Signature

*Please delete where inapplicable

Instruction:

Anyone who intentionally violates a rule in a university's examination regulations on cheating in examinations is committing a regulatory offence. This offence may be penalized with a fine of up to 50,000 euros. The administrative authority responsible for the prosecution and punishment of an offence is the Head of Administration (Kanzler) of TU Dortmund University. Furthermore, in case of a repeated or any other serious attempt to deceive, the examinee may be exmatriculated (§ 63 paragraph 5 Higher Education Act).

A willfully false declaration in lieu of oath may be punished with imprisonment of up to 3 years or a fine.

TU Dortmund University may use intellectual property verification tools (e.g. "turnitin") to check for regulatory offences in examination procedures.

I have noted the instructions given above:

Izmir, 01.06.2017

Place, date


signature